CHAPTER 31

Soft Magnetic Materials - Inductors and Transformers

Maxwell's equations form the basis of the relationships between the electrical and magnetic equations that are commonly used in the design of magnetic components such as inductors (choke, reactor) and transformers. The monogram below succinctly shows those relationships necessary for the design of magnetic components for power electronics applications.

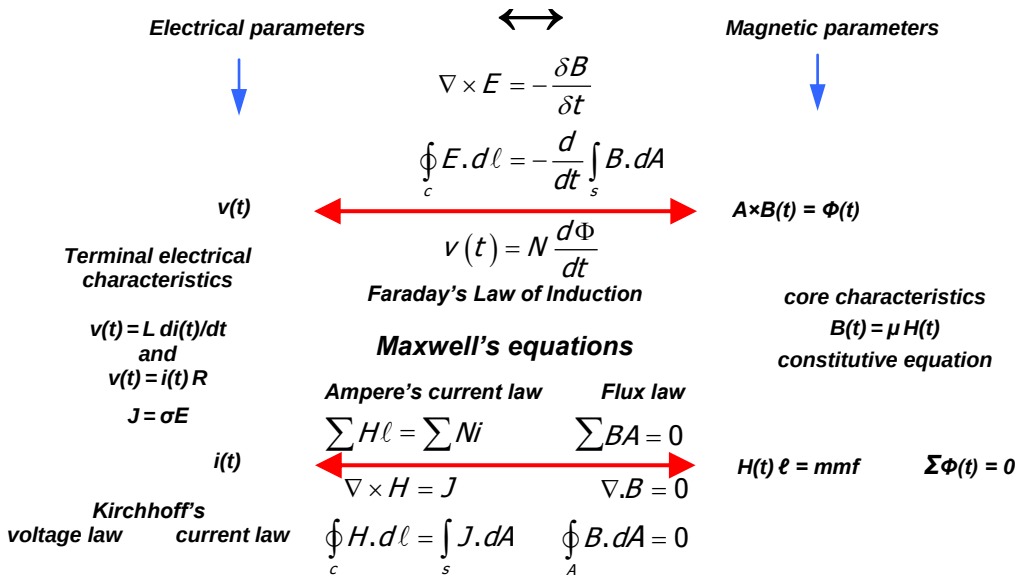

Soft magnetic materials (remove the field and the material returns to the non-magnetised state) are used extensively in power electronic circuits, as voltage and current transformers, saturable reactors, magnetic amplifiers, inductors, and chokes. These magnetic devices may be required to operate at only 50/60 Hz, or at frequencies down to dc or over 1 MHz. For example, a steel laminated ac mains voltage transformer operates at 50/60 Hz, while its ferrite switch-mode power supply counterpart may operate at 500 kHz. Soft magnetic materials have been utilised in other chapters for the following applications:

switching aid circuits	
- linear inductor	(9.3.3)
- saturable inductor	(9.3.4)
- snubber discharge	(figure 9.5)
- unified energy recovery	(10.2.1)
- thyristor *di/dt* control	(figure 9.5)
pulse transformers	(figures 8.7f)
current transformer	(Example 31.7)
turn-on snubber energy recovery	(figures 10.2a)
L-C resonator circuits	(figure 10.5c)
transient current sharing	(figure 11.8)
rfi filtering	(11.4.2)
single and three phase transformers	(22)
cycloconverter intergroup reactors	(15.5)
phase shifting transformers	(17.1.3ii)
current source inductors	(17.2)
smps inductance and transformers	(19, 20, 21)

Hard magnetic material devices, such as those materials used for permanent magnets and ferrite beads for rfi suppression, are considered in chapter 32.

31.1 Inductor and transformer electrical characteristics

Magnetic cores with windings form inductors (a single winding) and coupled circuits (more than one winding), namely transformers, as shown in figure 31.1. Typical *B-H* curve characteristics are shown in figure 31.2 for the different soft magnetic materials shown in Table 31.1.

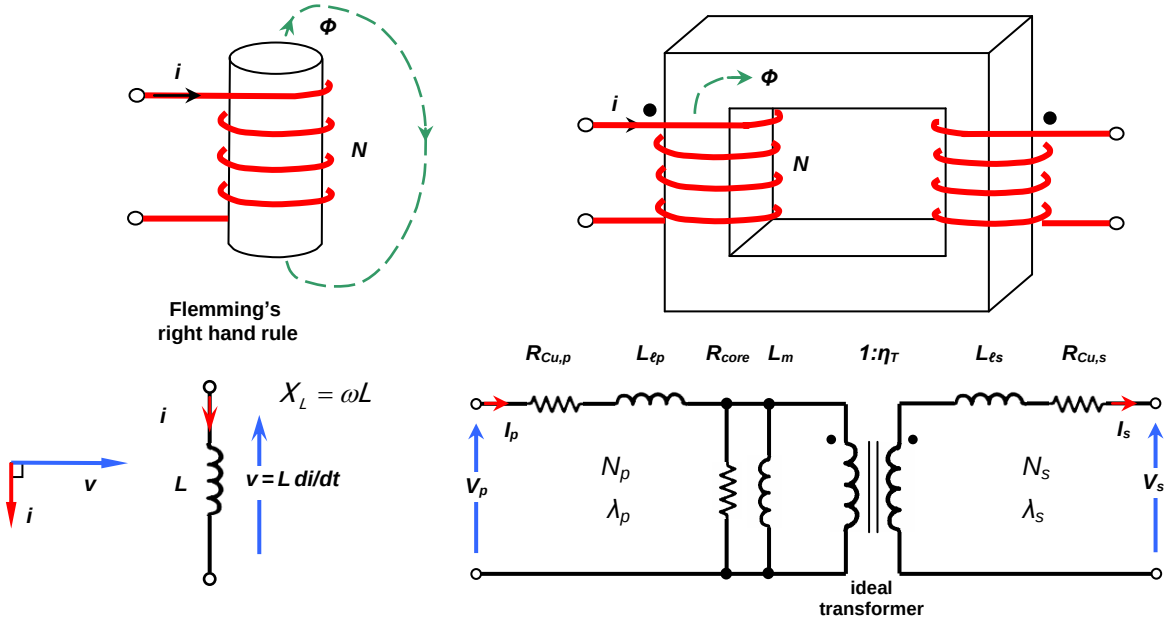

Figure 31.1. *Inductor and transformer models and circuits.*

31.1.1 Inductors

From Faraday's Law:

$$v = N\frac{d\phi}{dt} = NA\frac{dB}{dt} \qquad \text{(V)} \tag{31.1}$$

whence for sinusoidal flux

$$v = 4.44NB_sA_ef \qquad \text{(V)} \tag{31.2}$$

Inductance (specifically self-inductance) is specified from equation (31.1) and from

$$v = L\frac{di}{dt} \qquad \text{(V)} \tag{31.3}$$

$$L = N\frac{d\phi}{di} = N\frac{\Phi}{I} \qquad \text{(H)} \tag{31.4}$$

Using $\phi = BA_e$ and $H\ell_e = Ni$, equation (31.4) becomes

$$L = \frac{N^2A_e}{\ell_e}\,dB/dH \qquad \text{(H)} \tag{31.5}$$

where *dB/dH* is the slope of the *B-H* curve, according to $B = \mu_o\mu_i H$. Therefore, before core saturation

$$L = \frac{N^2A_e}{\ell_e}\mu_o\mu_i = \frac{N^2}{\Re} \quad \left(=\frac{N\Phi}{I}\right) \qquad \text{(H)} \tag{31.6}$$

where $\Re$ is the magnetic circuit reluctance.
The subscript ***e*** is used to denote the effective core parameter, as shown in Table 31.2.
The energy stored in an inductor is given by

$$W = \tfrac{1}{2}LI^2 \qquad \text{(J)} \tag{31.7}$$

The energy stored in an air gap volume is

$$W = \tfrac{1}{2}B^2\frac{A\ell_{ag}}{\mu_o} = \tfrac{1}{2}BH\,A\ell_{ag} \qquad \text{(J)} \tag{31.8}$$

while the force between the two magnetic surfaces bounding that air gap is

$$F = \tfrac{1}{2} B^2 \frac{A}{\mu_o} = \tfrac{1}{2} BH\ A \qquad \text{(N)} \tag{31.9}$$

The effective inductance of uncoupled series, L_s, and parallel, L_p, connected inductors are

$$\begin{aligned} L_s &= L_1 + L_2 + L_3 + \ldots \\ \frac{1}{L_p} &= \frac{1}{L_1} + \frac{1}{L_2} + \frac{1}{L_3} + \ldots \end{aligned} \tag{31.10}$$

31.1.2 Transformers or magnetically coupled circuits

The ideal transformer shown in figure 31.1, with a primary and a secondary winding, in the turns ratio 1:η_T, is wound so as to produce the shown voltages according to the usual flux dot convention. Any two of the following electrical equations can be used to derive the third equation (provided no energy is stored in the core).

$$\begin{aligned} P_{in} &= P_{out} \\ I_p \times 1 &= I_s \times \eta_T \\ \frac{V_s}{V_p} &= \frac{\eta_T}{1} \end{aligned} \tag{31.11}$$

Impedance in one winding can be referred (transferred) to the other winding in the turns ratio – squared. Series impedance Z_s in the secondary becomes $Z_p = Z_s / \eta_T^2$ in the primary circuit. Specifically

$$Z_s = R + j\omega L - \frac{1}{j\omega C} \quad \text{becomes} \quad Z_p = \frac{R}{\eta_T^2} + j\omega \frac{L}{\eta_T^2} - \frac{1}{j\omega \eta_T^2 C} \tag{31.12}$$

Note that secondary resistance and inductance referred to the primary are divided by the turns ratio squared, while capacitance is multiplied by η_T^2.

For mutually coupled circuits (transformers), the relationships between the primary and secondary flux linkages $\lambda = N\Phi$ and electrical parameters are

$$\begin{bmatrix} \lambda_p \\ \lambda_s \end{bmatrix} = \begin{bmatrix} L_p & L_{12} \\ L_{21} & L_s \end{bmatrix} \begin{bmatrix} i_p \\ i_s \end{bmatrix} \qquad \begin{aligned} v_p &= L_p \frac{di_p}{dt} \pm M \frac{di_s}{dt} \\ v_s &= L_s \frac{di_s}{dt} \pm M \frac{di_p}{dt} \end{aligned} \tag{31.13}$$

where L_s and L_p are the primary and secondary self inductances given by any of equations (31.4) to (31.6).

M is the mutual inductance, $M = k\sqrt{L_p L_s} = k\ N_s \frac{\Delta\phi}{\Delta i_p}$ for a coupling factor k ($0 \le k \le 1$).

The stored magnetic energy in the core with current in the primary and secondary is

$$\begin{aligned} W &= \tfrac{1}{2} L_p i_p^2 \pm M i_p i_s + \tfrac{1}{2} L_s i_s^2 \\ &= \tfrac{1}{2} \left(\sqrt{L_p}\, i_p \pm \sqrt{L_s}\, i_s \right) \end{aligned} \tag{31.14}$$

In equation (31.14), it is required for a transformer, that no energy is stored in the core whence the negative sign is applicable and for energy $W = 0$, $1 \times i_p = \eta_T \times i_s$. Faraday's Law, equation (31.2), is applicable to transformers. In the case of a transformer, this equation shows that the advantage of a high core flux density is that more volts v, per turn N, for a given frequency f, results.

When the primary and secondary coupled coils are series connected

$$L_{series} = \left(L_p \pm M \right) + \left(L_s \pm M \right) = L_p + L_s \pm 2M \quad = \left(N_p + N_s \right)^2 / \Re \tag{31.15}$$

When the primary and secondary coils are parallel connected

$$L_{parallel} = \frac{1}{L_p \pm M} + \frac{1}{L_s \pm M} = \frac{L_p \times L_s}{L_p + L_s \pm 2M} \tag{31.16}$$

Note the extra mutual coupling terms, when compared to equation (31.10) for the uncoupled cases.

Figure 31.1 shows how the coupled circuit model of the ideal transformer, is extended to give the usual transformer model, which includes copper winding resistance R_{Cu}, leakage inductance L_ℓ, magnetising inductance L_m, and core losses (eddy current and hysteresis) R_{core}.

31.2 Magnetic material types

Diamagnetic ($\mu_r < 1$) and paramagnetic ($\mu_r \gtrsim 1$) materials are not considered. Two basic types of soft magnetic materials are common, depending on the application requirements. These materials are:

- Ferromagnetic materials based on iron and nickel, which are for lower frequencies, < 2kHz, while
- Ferrimagnetic materials (a subgroup of ferromagnetic materials), which are based on ceramic oxides of metals (ferrites), are applicable to frequencies from a few kilohertz to well over 80 MHz.

31.2.1 Ferromagnetic materials

31.2.1i - Steel

Cold-rolled grain-oriented steel is a 3-4 per cent silicon iron, cold reduced to develop a high degree of grain orientation, which gives

- increased flux for a given magnetising force and
- decreased size for a given rating, hence reduced weight.

Normally cores are produced in a number of material lamination thicknesses

- 0.3 mm for frequencies up to 200 Hz
- 0.1 mm for frequencies between 200 Hz to 2 kHz and
- 0.05 mm for higher frequencies and pulse applications.

Steel laminations for low frequency applications are available in different shapes. E and I laminations or strip C cores or toroids are extensively used for mains transformers and ac line inductors. Non-orientated silicon steels are extensively used for machine laminations.

31.2.1ii - Iron powders

Two general forms of iron powder cores are employed

- Cores are made by highly compacting insulated high quality spongy iron powder.
- High resistivity is required to reduce eddy current losses, so the iron powder is subjected to an acid treatment to produce an insulating oxide layer on the surface of each individual particle. This fine carbonyl iron is mixed with a bonding material and highly compressed. The bonding material used limits the maximum core temperature. Minute gaps appear between the particles, severely reducing the permeability. It is difficult to saturate such materials.

31.2.1iii - Alloy powders

These cores are made by highly compacting insulated alloy powder. The alloy is usually 50-75 per cent nickel, the remainder being iron with a small percentage of copper and molybdenum. The higher the iron percentage, the higher the saturation flux density and the higher the core losses.
Powder iron and alloy cores are available in toroidal or ring shapes, cylindrical and hollow cylindrical cores, as well as cup cores, bobbins, pot cores, and beads.

31.2.1iv - Nanocrystalline

Nanocrystalline soft magnetic alloys are brittle, thin ribbon 18μm thick, materials based on iron Fe, silicon Si and boron B with small additions of niobium Nb and copper Cu. They are produced via a rapid solidification technique, being initially in a precursor amorphous (non-crystalline) state and then crystallized into a precise mix of amorphous and nanocrystalline phases when subsequently heat annealed at around 500 to 600°C.
An amorphous magnetic metal has high permeability due to no crystalline magnetic anisotropy. However when applying heat treatment on a typical amorphous metal at temperatures higher than its crystalline temperature, magnetic properties deteriorate for a rapid crystal growth of grains up to 1um. But if the recrystalline grains are restricted to the nano-order, about 10 nm in size, the soft magnetic crystal grains have good magnetic properties. Thus the suppressed grain growth recrystalization during annealing due to the enriching Nb and Cu gives the material its unique magnetic properties. This extremely fine-grained microstructure with grain sizes of 10 nanometres is termed nanocrystalline.
Nanocrystalline alloys combine low magnetic anisotropy and low magnetostriction, both prerequisites for high magnetic permeability, with high magnetic flux density B_s and good thermal stability. Due to the exchange coupling of randomly oriented grains of Fe, the magnetocrystalline anisotropy averages out to zero. Magnetostriction can also be cancelled by a combination of positive values for the crystalline phase and negative values for the remaining amorphous phase, resulting in zero magnetostriction.

Figure 31.2a shows permeability and saturation magnetic flux densities of representative nanocrystalline soft magnetic materials. Since the compositions of nonmagnetic elements can be reduced in the alloy design, higher saturation magnetic flux density can be obtained in the nanocrystalline soft magnetic materials compared to the existing bulk soft magnetic and amorphous materials.

31.2.2 Ferrimagnetic materials - soft ferrites

Ferrites are grey/black, hard, brittle, chemically inert ceramic materials, which have a magnetic cubic (spinel) structure of 10 to 20μm crystals containing the aligned Weiss domains.
The most general ferrites are polycrystalline magnetic isotropic (grains non-aligned) ceramic oxides, which are compounds of iron oxide, Fe_20_3, about 50%, mixed with one or more oxides of bivalent transition metals, Me, such as Fe0, Ni0, Zn0, Mn0, Cu0, Ba0, Co0, and Mg0, to give the general compositional form $MeFe_20_4$. At lower frequencies, below a few MHz, a Mn-Zn combination is added to iron oxide, while for higher frequencies, above a MHz, Ni-Zn is the additive.
The raw pure oxide or carbonates materials of the constituent metals are mixed with organic binders, pre-sintered at 1000°C, a process called Calcining and then the partially formed ferrite structure pellets are wet ground by milling, to form a submicron particle slurry with water. After spray drying, the powder material is shaped by means of pressing and sintering at between 1150°C and 1300°C, which cause densification and substantial shrinkage. The sintering process involves raising the temperature to 1300°C in about 3 hr, with 15 per cent oxygen present. The cores are cooled slowly without oxygen present to about 200°C in 20 hr after entry. In producing the ferrite crystal structure, a 15 per cent linear, and 40 per cent by volume shrinkage occurs during sintering.
A diverse range of ferrite core shapes is available, which include, E, I, U, toroid, drum, pot, rod, tube, and screw. Where appropriate, diamond-wheel-ground air gaps are available on the centre pole. Manufacturing yields limit the physical component in size. Toroid cores of 152 mm outside diameter are not uncommon, and exotic shapes such as motor stators are made for special applications.

31.3 Comparison of material types

Table 31.1 shows typical comparative data for the main classes of soft ferro and ferri magnetic materials. Generally, those materials with higher saturating flux densities, B_s, have higher initial permeability μ_i, and hence offer higher inductance but at the expense of higher core eddy current and hysteresis losses.

Table 31.1: Typical comparative data of soft magnetic materials

Material	thickness	B_s	B_r / B_s	H_c	μ_r	μ_r	P_{cv}	λ_s	T_c
	μm	T	%	A/m	$\times 10^3$ 1kHz	$\times 10^3$ 100kHz	kW/m^3	10_6^-	°C
		H_m=800A/m 25°C	H_m=800A/m 25°C	H_m=800A/m 25°C	H_m=0.5A/m 25°C	H_m=0.5A/m 25°C	100kHz B_m=0.2T 25°C		
Nanocrystalline Square Fe-Si	18	1.23	89	0.6	30	5	600	0	570
Nanocrystalline hi-μ_r Fe-Si	18	1.23	5	0.6	50	16	250	0	570
Fe based amorphous	25	1.56	83	2.4	5	5	2200	+27	415
Co-based hi-μ_r amorphous	20	0.55	5	0.3	115	18	280	0	180
Co-based square amorphous	20	0.60	85	0.3	30	10	460	0	210
3% Si steel	50	1.9	85	6.0	2.7	0.8	8400	-0.8	750
6½% Si steel	50	1.3	63	45	1.2	0.8	5800	-0.1	700
50% Ni Permalloy	25	1.5	95	12	-	-	3400	+25	500
80% Ni hi-μ_r Permalloy	25	0.74	55	0.5	50	5	1000	0	480
80% Ni square Permalloy	25	0.74	80	2.4	-	-	1200	0	460
Mn-Zn hi-μ_r ferrite	-	0.44	23	8.0	5.3	5.3	1200	-0.6	150
Mn-Zn low-loss ferrite	-	0.49	29	12	2.4	2.4	680	-0.6	220

In rfi suppression and filtering applications, silicon steel is not effective since the initial permeability, μ_i, falls rapidly with frequency hence at the high suppression frequency, inductance is small. Thus iron powder or a high iron alloy may be used, which have relatively high flux densities and high losses. For rfi suppression, a high core loss aids suppression at the expense of linearity.
At inaudible frequencies, >20 kHz, for a low core loss, ferrites are extensively used. Although ferrite flux densities are relatively low, typically 0.5 T for power application ferrites, eddy current and hysteresis losses are low. The low eddy current loss results from the high core material resistivity. With ferromagnetic materials, the eddy current loss is reduced by using thinner laminations or electrically isolated powder particles. A major disadvantage of a ferrite core is its poor temperature stability and low allowable core temperature. On the other hand, high initial permeabilities, >20,000, are obtainable.
Ferrite materials, application, and component design are specifically considered, although the concepts developed are generally applicable to ferromagnetic materials.

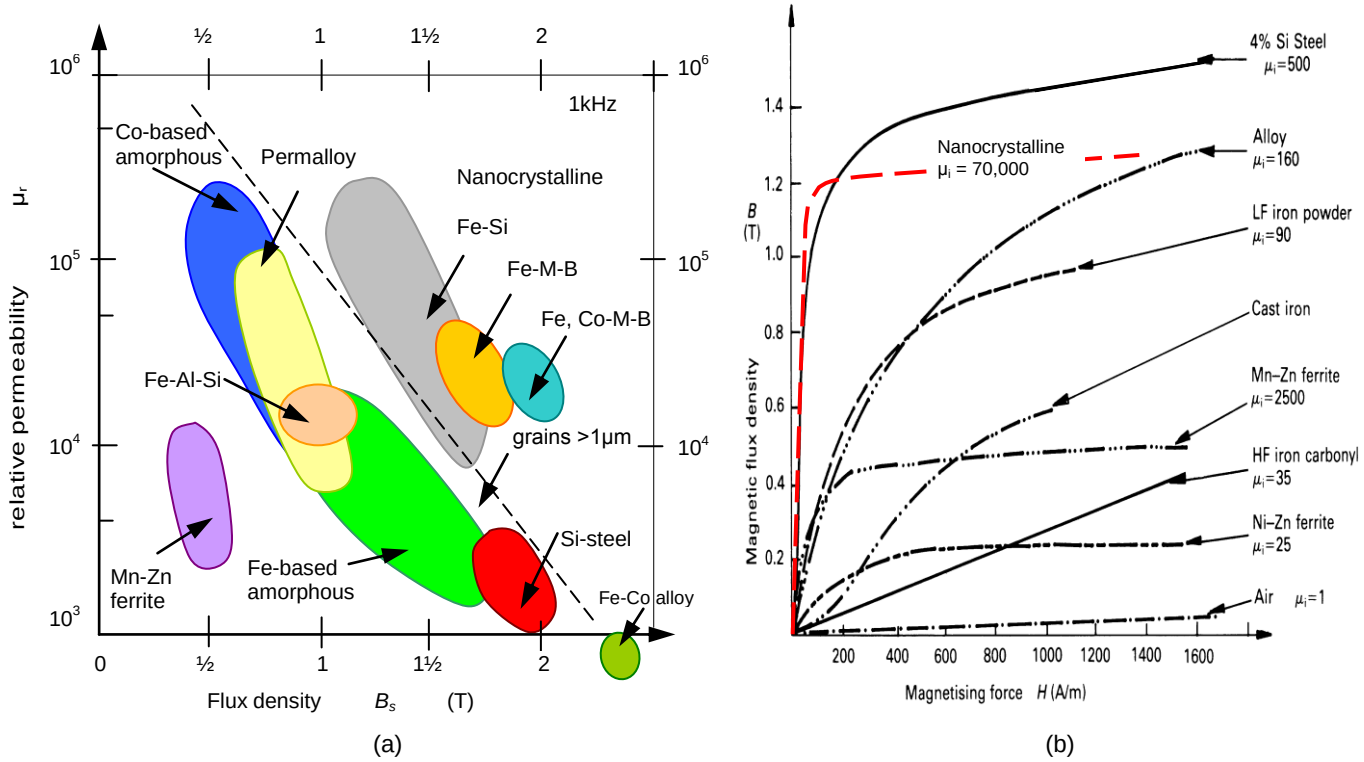

Figure 31.2. *Magnetic alloy characteristics:*
(a) permeability versus saturation magnetic flux densities and (b) B-H characteristics.

31.4 Ferrite characteristics

The definitions and explanations given are applicable to soft magnetic materials in general, and are illustrated specifically by reference to ferrite materials.
General mechanical and thermal properties of power ferrites are given in Appendix 31.7, while typical magnetic properties are given in Appendix 31.8.

Table 31.2: Core effective magnetic dimensions and parameters

core factor	symbol	definition	units
form factor, ℓ_e/A_e	c_1	$\Sigma\ell/A$	m^{-1}
effective magnetic area	A_e	$c_1/\Sigma\ell/A^2$	m^2
effective magnetic length	l_e	$A_e\,c_1$	m
effective magnetic volume	V_e	$\ell_e\,A_e$	m^3
core permeance	c	μ_o/c_1	H

31.4.1 Dimensions and parameters

The effective magnetic dimensions are constant for a given core and are defined in Table 31.2. These effective constants are based on the length ℓ and area A of the individual limbs comprising the complete

core. These effective dimensions are used for magnetic component design, such as transformer core loss, which is given per unit effective volume, V_e.
From the parameters in Table 31.2, inductance is calculated from equation (31.6) as

$$L = \mu_i c N^2 \qquad \text{(H)} \tag{31.17}$$

31.4.2 Permeability

Figure 31.2 shows that a non-linear relationship exists between B and H for magnetic materials, and is characterised by the dimensionless parameter μ_r - the relative permeability - according to $B = \mu_o \mu_r H$ (where $\mu_o = 4\pi \times 10^{-7}$ H/m). Figure 31.3 shows a detailed B-H magnetising curve for a ferrite material along with its hysteresis loop. The case of an air core magnetic circuit, for which $\mu_r = 1$, is also shown.
Figure 31.3 illustrates various definitions for μ_r based on the ratio flux density to field strength, namely

$$\mu_r = \frac{1}{\mu_o}\frac{B}{H} \tag{31.18}$$

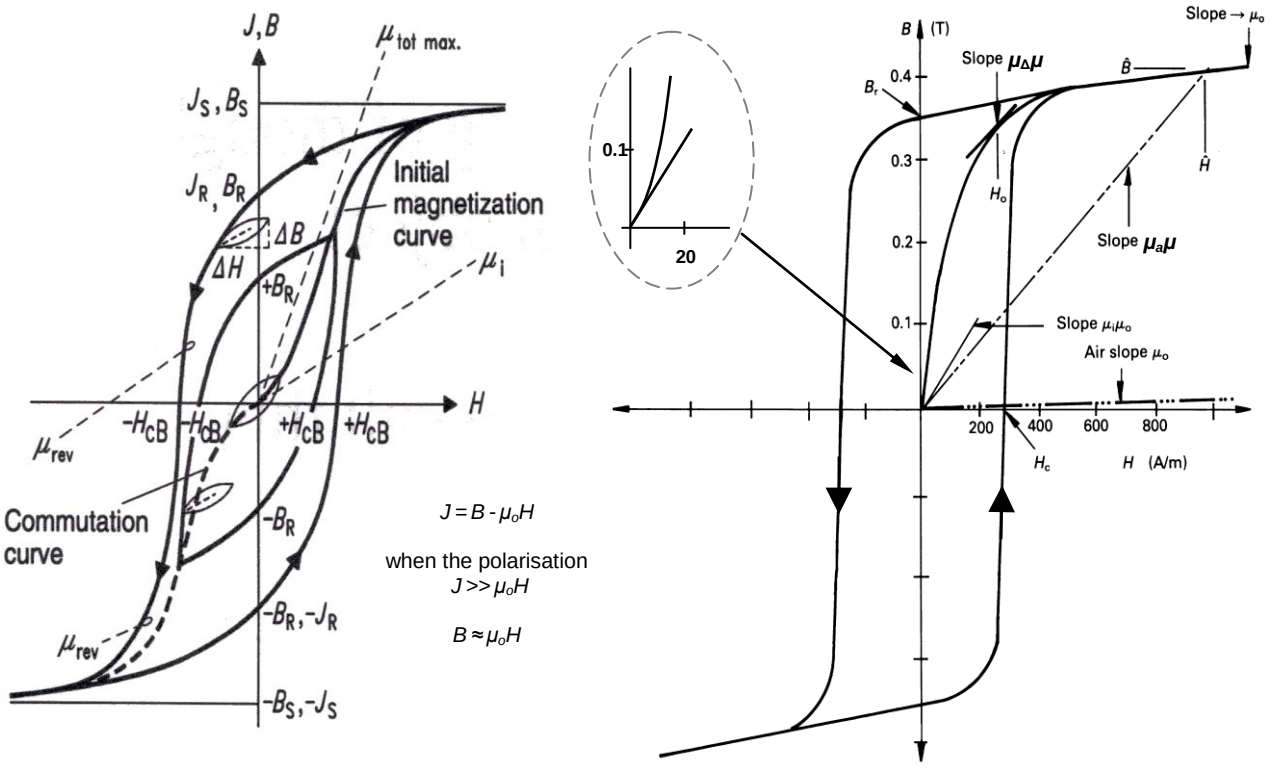

Figure 31.3. *Hysteresis loop illustrating permeability definitions, remanence B_r, and coercive force H_c.*

31.4.2i *- Initial or intrinsic permeability, μ_i*

The initial permeability, which is dependent on temperature and frequency, is the permeability at weak field strengths at $H = 0$ and ΔH tends to zero, that is

$$\mu_i = \frac{1}{\mu_o}\left[\frac{\Delta B}{\Delta H}\right]_{H = 0,\ \Delta H \to 0} \tag{31.19}$$

31.4.2ii *- Amplitude permeability, μ_a and maximum permeability, $\hat{\mu}$*

The amplitude permeability applies to large magnitude sinusoids (high excitation), with no dc field (offset) applied, and is the ratio of the sinusoid peak B and H

$$\mu_a = \frac{1}{\mu_o}\left[\frac{\hat{B}}{\hat{H}}\right]_{H = 0} \tag{31.20}$$

The maximum permeability $\hat{\mu}$ is the maximum μ_a obtainable for any H, that is, $\hat{\mu}$ = max [μ_a] for all values of H. The variation of amplitude permeability with magnetising force or flux density is shown in figure 31.4. Because of the non-linear nature of the B-H curve loop, the amplitude permeability is highly dependant on the applied field strength magnitude. The figure 31.4 is representative of a ferrite material suitable for a wide range of power electronic applications. More technical data for this material is presented in Appendix 31.8 and in the figures that follow.

31.4.2iii *- Reversible or incremental permeability, μ_{rev}, μ_Δ*

When a core is magnetised with a polarising dc offset field upon which a small ac field is superimposed, the ac *H* field produces a small lancet-shape hysteresis loop which reduces to a straight line as the ac *H* field is reduced. The slope of this line, shown in figure 31.3, is the incremental or reversible permeability

$$\mu_\Delta = \frac{1}{\mu_o}\left[\frac{\Delta B}{\Delta H}\right]_{H\ =\ \text{constant}} \qquad \mu_{rev} = \frac{1}{\mu_o}\lim_{\Delta H \to 0}\left[\frac{\Delta B}{\Delta H}\right]_{H\ =\ \text{constant}} \tag{31.21}$$

The incremental permeability, μ_Δ is a function of the dc magnetic bias, as shown in figure 31.5. It is usually a maximum when no dc field is present, while for a toroid it is identical to the initial permeability, μ_i. With increased current, μ_Δ, hence inductance, decreases. The reversible permeability is when $\Delta H \to 0$.

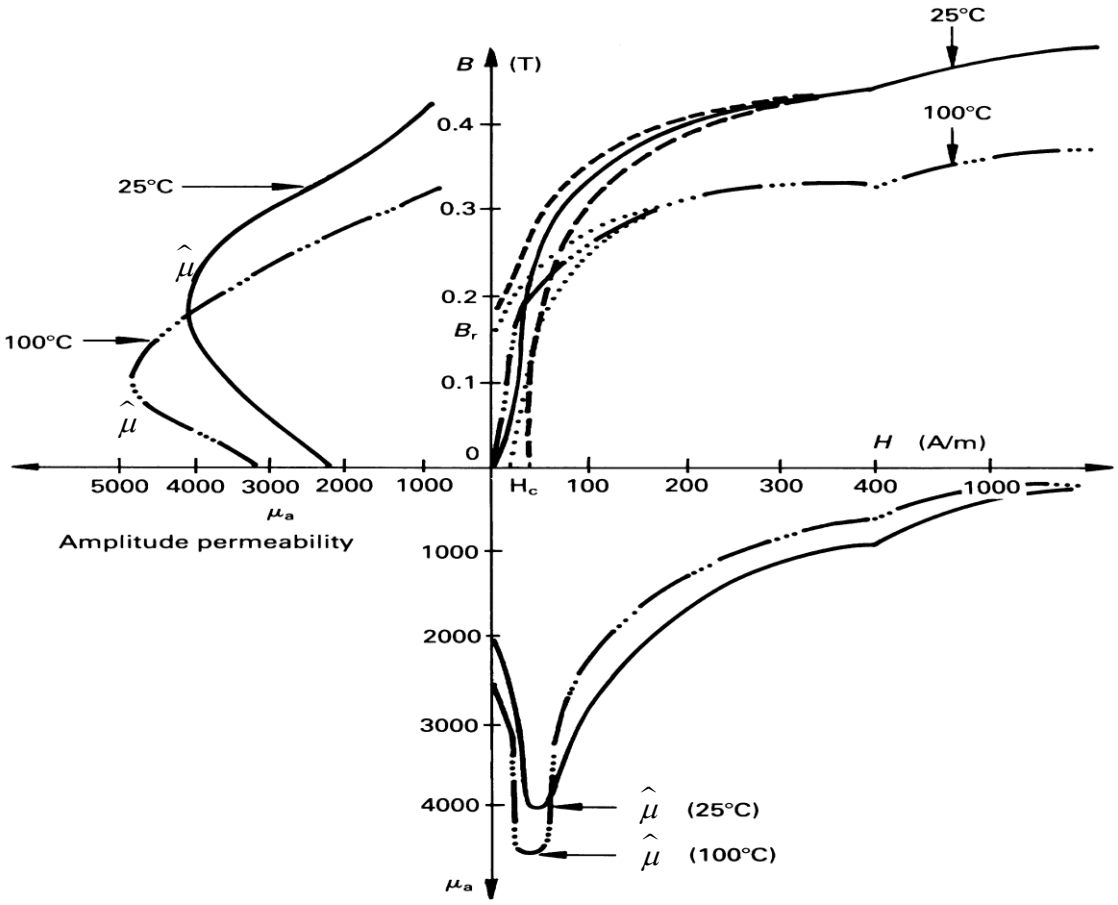

Figure 31.4. *Temperature dependence of flux density B and amplitude permeability, μ_a.*

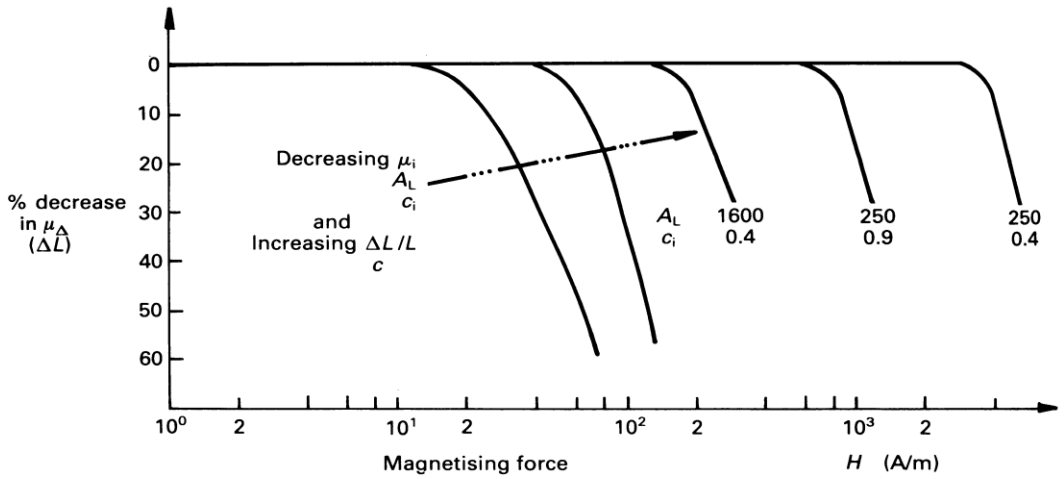

Figure 31.5. *Variation of permeability with field strength.*

31.4.2iv - *Effective permeability, μ_e*

The inductance of a coil with a (air) gapped core of effective (or apparent) permeability μ_e is given by

$$L = \frac{\mu_o \mu_e N^2}{\sum \ell / A} = \mu_e c N^2 = A_L N^2 = \mu_e L_o \qquad \text{(H)} \tag{31.22}$$

hence

$$\mu_e = \frac{L}{cN^2} = \frac{L}{L_o} = \frac{1}{\mu_o}\frac{L}{N^2}\sum \ell / A \tag{31.23}$$

where L_o is the coil inductance if the core is removed (air, μ_r=1), whence the permeability drops. The term A_L is the inductance factor and is equal to $\mu_e c$. Conversely

$$N = \alpha\sqrt{L} \tag{31.24}$$

where $\alpha = 1/\sqrt{A_L}$ and is termed the turns factor.

If the air gap width, ε, is small compared with the core of effective length, ℓ_e, such that $\varepsilon << \ell_e$, the effective permeability approximates to

$$\frac{1}{\mu_e} = \frac{1}{\mu} + \frac{\varepsilon}{\ell_e} \tag{31.25}$$

The introduction of an air gap is equivalent to connecting two inductors in parallel: one without an air gap, μL_o; the other also without a gap but having an inductance $(\ell_e/\varepsilon)\, L_o$. The effective permeability of a gapped core at low flux levels is specified by the initial permeability, μ_i, and is given by

$$\frac{1}{\mu_e} = \frac{1}{\mu_i} + \frac{\varepsilon}{\ell_e} \tag{31.26}$$

The effective permeability for high flux densities is expressed in terms of the amplitude permeability, μ_a, that is

$$\frac{1}{\mu_e} = \frac{1}{\mu_a} + \frac{\varepsilon}{\ell_e} \tag{31.27}$$

That is

$$\mu_e = \frac{\mu_a}{1 + \frac{\varepsilon\,\mu_a}{\ell_e}} \tag{31.28}$$

If the magnetic circuit is not homogeneous, has an air gap for example, the effective permeability is the permeability of an equivalent homogeneous non-gapped structure of the same shape, dimensions, and reluctance that would give the inductance equivalent to the gapped structure.

A fringing factor, ε/β, must be introduced for significant gap widths, to account for the effective increase in permeability due to the fringing flux effect. The bulging flux in the gap results in a reduced gap flux density since the effective gap area is increased.

31.4.2v - *Complex permeability, $\bar{\mu}$*

Because of core losses, a coil can be represented by

- a series L_s - R_s circuit for an inductor, figure 31.6 (and for the characterisation of ferrites)
- a parallel $R_p \,//\, L_p$ circuit for a transformer (magnetically coupled circuit), figure 31.6.

Core losses are modelled by the inclusion of resistance and the associated losses can be accounted for by considering the coil permeability as a complex variable, $\bar{\mu}$. For the inductor series equivalent circuit

$$Z = R_s + j\omega L_s = j\omega\bar{\mu} c N^2 = j\omega\bar{\mu} L_o = \omega L_o \mu_s'' + j\omega L_o \mu_s' \qquad (\Omega) \tag{31.29}$$

where $L_o = c N^2$ (μ_s'' and μ_s' are the real (inductance) and imaginary (loss) components of $\bar{\mu}$) such that

$$\begin{aligned} \bar{\mu} &= \mu_s' - j\mu_s'' \\ &= \frac{L_s}{cN^2} - j\frac{R_s}{\omega c N^2} \end{aligned} \tag{31.30}$$

while for the transformer parallel equivalent circuit (figure 31.6)

$$\frac{1}{Z} = \frac{1}{R_p} + \frac{1}{j\omega L_p} = \frac{1}{\omega\mu_p'' L_o} - \frac{1}{j\omega\mu_p' L_o} = \frac{1}{j\omega\bar{\mu} L_o} \qquad \text{(S)} \tag{31.31}$$

such that

$$\begin{aligned} \frac{1}{\bar{\mu}} &= \frac{1}{\mu_p'} - \frac{1}{j\mu_p''} \\ &= \frac{1}{L_p / cN^2} - \frac{1}{jR_p / \omega c N^2} \end{aligned} \tag{31.32}$$

Since the parallel and series circuits are equivalent

$$\frac{\mu_s''}{\mu_s'} = \frac{\mu_p'}{\mu_p''} = \tan\delta \tag{31.33}$$

where tan δ is the core loss factor (deviation from the ideal phase angle of 90°)

$$\tan\delta = \frac{R_s}{\omega L_s} = \frac{\omega L_p}{R_p} = \frac{1}{Q} \qquad \left(= \frac{\mu_s''}{\mu_s'} = \frac{\mu_p'}{\mu_p''}\right) \tag{31.34}$$

Q is a measure of the efficiency of the magnetic component.
The complex permeability components are related according to

$$\begin{aligned} \mu_p' &= \mu_s'\left(1+\tan^2\delta\right) = \mu_s'\left(1+{}^{1}\!/_{Q^2}\right) \\ \mu_p'' &= \mu_s''\left(1+{}^{1}\!/_{\tan^2\delta}\right) = \mu_s''\left(1+Q^2\right) \end{aligned} \tag{31.35}$$

The parallel and series equivalent components are related by

$$\begin{aligned} R_s &= \frac{R_p}{1+Q^2} = \frac{R_p}{1+{}^{1}\!/_{\tan^2\delta}} \\ L_s &= \frac{L_p}{1+{}^{1}\!/_{Q^2}} = \frac{R_p}{1+\tan^2\delta} \end{aligned} \tag{31.36}$$

The phasor diagram for the equivalent parallel and series inductor models are shown in figure 31.6.

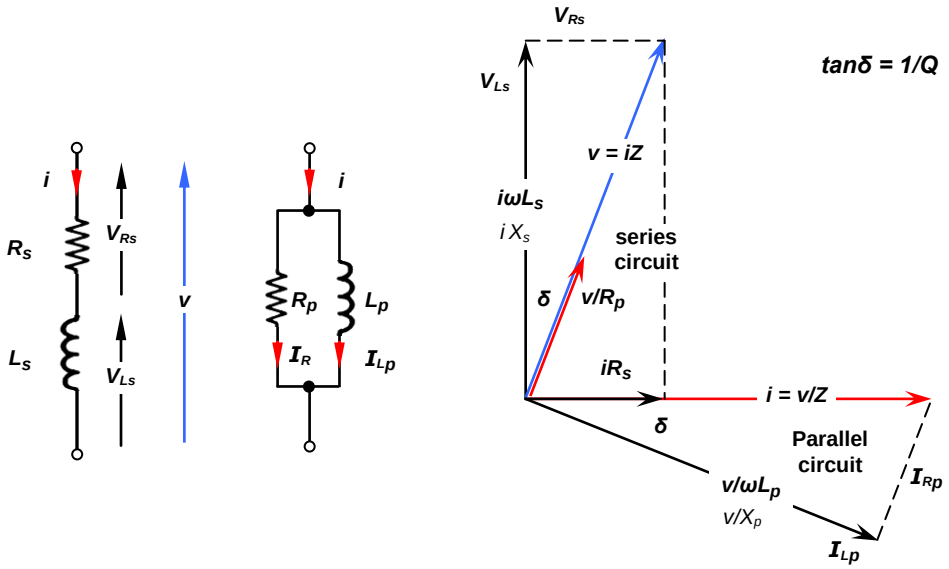

Figure 31.6. *Inductor parallel and series equivalent circuit vector diagrams.*

For low losses, namely at low frequencies, $\tan^2\delta \to 0$ in equation (31.35), whence $\mu_p' = \mu_s'$, while at high losses, at high frequencies, $\mu_p'' = \mu_s''$ since $\tan^2\delta \to \infty$ in equation (31.35). Complex permeability characteristics are shown in figure 31.7. The cut-off frequency, f_c is defined as the frequency at which the permeability is half the initial permeability, μ_s', at low frequency. At 25°C, f_c for Mn-Zn materials is approximated by $f_c \approx 4000/\mu_i$ (MHz), for μ_i at low frequency.

The complex permeability components are measured at low flux densities. Mn-Zn ferrites applicable to power application usually have high permeability, modest resistivity, and a high dielectric constant. In such cases, the complex permeability is highly dependent on the core dimensions, as shown in figure 31.7, which characterises stacked toroids. Because of the associated large volume, volume resonance occurs where eddy currents dominate losses.

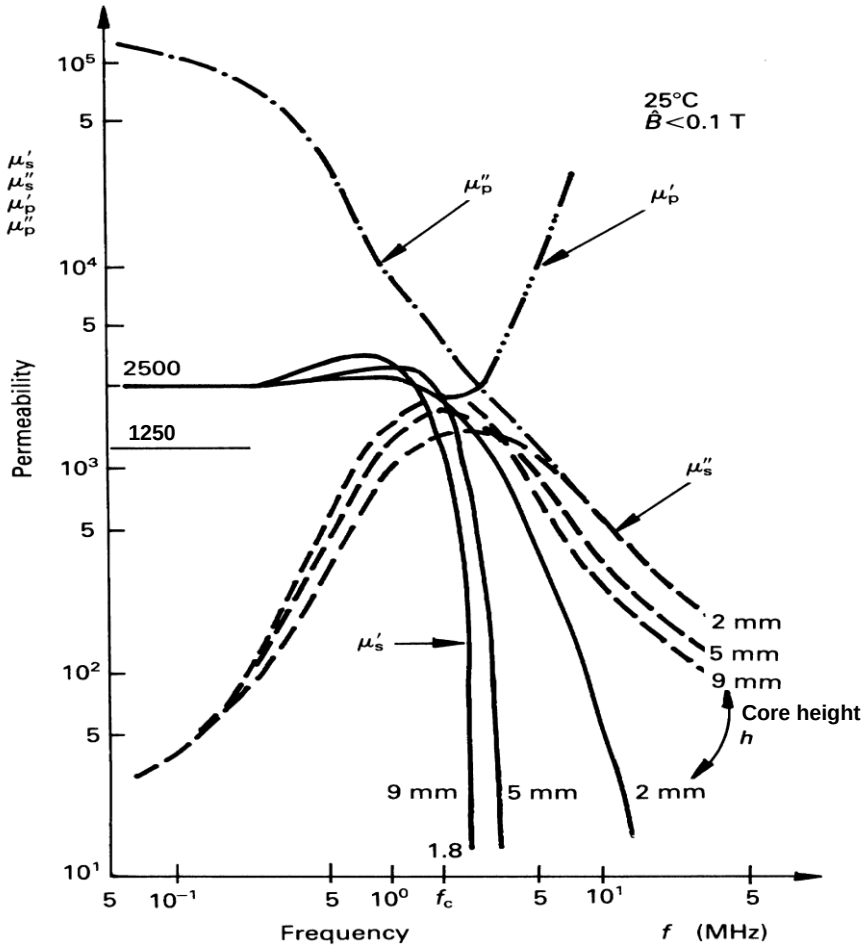

Figure 31.7. *Influence of core height (h) on the frequency characteristics of the complex permeability for a toroid.*

31.4.3 Coercive force and remanence

The coercive force H_c is the field strength at which the hysteresis loop cuts the *H*-axis as shown in figures 31.3 and 31.4. It is the reverse magnetic field needed to reduce a magnetically saturated structure from remanence to zero magnetic induction. It is representative of the static hysteresis loss of the material. The point where the hysteresis loop intersects the *B*-axis is called the remanence (flux density), B_r. Where a core is operated with a magnetic field strength bias, for example, as with an inductor carrying dc current, the value of flux density is reduced to B_s - B_r for calculations. The area within the hysteresis loop represents core hysteresis loss, in Joules per unit volume.

31.4.4 Core losses

31.4.4i *- Core losses at low H*

At low magnetising forces, the total losses, represented by R_t, can be separated into three core components (magnetic components, R_m) and a copper turns component, R_{Cu}. The components are

- frequency dependent eddy currents, R_F
- frequency dependent hysteresis, R_h
- magnetic drag, remanence loss, or residual loss, R_r
- copper winding loss including both dc and ac components, R_{Cu}, where

$$R_t = R_{Cu} + R_m$$
$$R_t = R_{Cu} + R_F + R_h + R_r \qquad (\Omega) \tag{31.37}$$

The coil is represented by the series R_t - L_s circuit where L_s is the lossless self-inductance. Empirical formulae, called *Jordan formulae* can be used to calculate R_t at low magnetic forces.

The series coil model impedance is given by (equation (31.29))

$$Z = R_t + j\omega L_s \qquad (\Omega) \tag{31.38}$$

whence

$$\tan\delta_t = R_t \big/ \omega L_s = R_{Cu} + R_m \big/ \omega L_s \qquad = \frac{R_{Cu}}{\omega L_s} + \frac{R_F}{\omega L_s} + \frac{R_h}{\omega L_s} + \frac{R_r}{\omega L_s} \tag{31.39}$$

$$= \tan\delta_{Cu} + \tan\delta_{mu} = \tan\delta_{Cu} + \tan\delta_F + \tan\delta_h + \tan\delta_r$$

where tan δ_t is the loss factor for the coil (which includes the core component tan δ_m). The reciprocal of the loss factor is the inductor quality factor, namely

$$Q = \frac{1}{\tan\delta_t} = \frac{\omega L_s}{R_t} \tag{31.40}$$

The copper loss (R_{Cu}) is usually excluded so as to characterise the core material specifically, whence

$$Q = \frac{1}{\tan\delta_m} = \frac{\mu_s''}{\mu_s'} = \frac{\mu_p'}{\mu_p''} \tag{31.41}$$

An alternative relative core loss factor is tanδ_m /μ_i or 1/ $\mu_i Q$. This particular figure of merit factor is generally characterised only for high frequency Ni-Zn ferrites. The relative loss factor for a gapped core, tan δ_e, assuming the various relative permeabilities are much greater than 1, can be found by multiplying the core loss factor by the gapped core effective permeability, μ_e, that is

$$\tan\delta_e = \frac{\mu_e}{\mu}\tan\delta \tag{31.42}$$

The term μ_e/μ_i is extensively used in equations to account for an air gap introduced into the core length. In transformers, the hysteresis component R_h increases as the hysteresis loop opens up at higher flux densities, and the hysteresis loss resistance R_h, in terms of the hysteresis loss factor tanδ_h, is

$$R_h = \omega L \times \tan\delta_h$$

The hysteresis material constant η_B, which characterises hysteresis losses of a specific material at higher flux densities, is

$$\eta_B = \frac{\tan\delta_h}{\mu_e \times \Delta\hat{B}}$$

31.4.4ii *- Core losses at high H*

1 - Ferrites

Core losses, P_V, with high flux densities in Mn-Zn ferrites are applicable to power electronic application. Empirical formulae are not practical, and ferrites used for choke and transformer cores are provided with experimentally characterised total core loss per unit volume data, as indicated in figure 31.8. This loss, for a power Mn-Zn ferrite, is given as a function of frequency, temperature, and flux density. The general loss term for hysteresis and eddy current losses is of the form

$$P_v = k f^a B^b \qquad (\text{W/m}^3) \tag{31.43}$$

where $1.2 < a < 1.6$ for hysteresis loss and $1.9 < a < 2.2$ for eddy current loss
$2.1 < b < 2.6$ for hysteresis loss and $1.8 < b < 2.3$ for eddy current loss
k is a function of temperature

For a specified and limited operating range, core losses in figure 31.8 can be approximated by

$$P_V(25°\text{C}) = P_h + P_F$$

$$= 5.8\times10^{-5}\times f^{1.2}\times\hat{B}^{2.11} + 3.32\times10^{-7}\times f^2\times\hat{B}^2 \qquad (\text{mW/cm}^3) \tag{31.44}$$

where f is in kHz for 10 kHz ≤ f ≤ 500 kHz

and $\hat{B}$ is the peak flux density in mT for 50mT ≤ $\hat{B}$ ≤ 250mT.

Temperature dependence is modelled according to

$$P_V = \kappa \times P_V(25°\text{C}) \tag{31.45}$$

where

$$\kappa = 1.48\times10^{-4}\times T^2 - 21.2\times10^{-3}\times T + 1.44$$

for f < 200 kHz and $\hat{B}$ ≥ 100 mT

$$\kappa = 1.2\times10^{-4}\times T^2 - 17.8\times10^{-3}\times T + 1.38$$

for f ≥ 200 kHz and $\hat{B}$ ≤ 100 mT

The temperature T is with respect of 0°C.
The per unit volume loss $P_V(T)$ is applicable to a square wave. For a half wave sine, power losses are reduced by 0.7 - 0.8 while for a full wave rectified sine wave, losses are increased by 1.8 to 2.2.

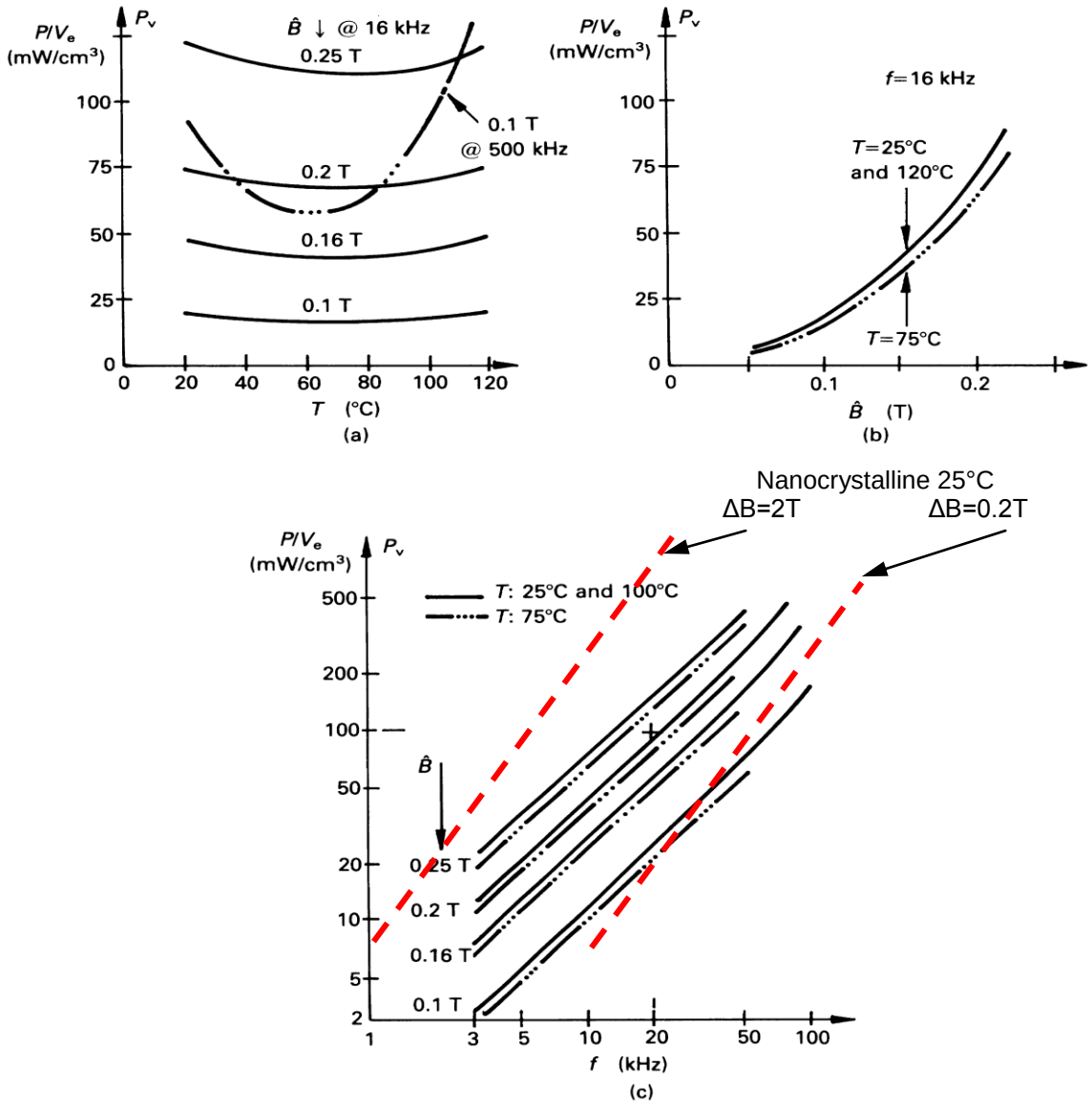

Figure 31.8. *Total per unit volume core losses as a function of: (a) core temperature, T; (b) maximum flux density, $\hat{B}$; and (c) frequency, f.*

2 - Nanocrystalline alloys

The magnetic reversal loss characteristics of nanocrystalline material is similar to that of ferrite, but with lower losses, higher permeability, higher operating temperatures, and higher allowable flux swings. Based on equation (31.43), core losses are approximated by

$$P_v = 3.09 \times \Delta B^{1.5} \times f^{1.5} \qquad \left(\text{mW/cm}^3\right) \tag{31.46}$$

Since the density is 7.35 g/cc, that is 1W/kg=7.35mW/cm^3

$$P_v = 0.42 \times \Delta B^{1.5} \times f^{1.5} \qquad \left(\text{W/kg}\right) \tag{31.47}$$

These empirical formula, shown in figure 31.8c, are valid for flux swings of up to $\Delta B = 2\text{T}$ and $f \le 200\text{kHz}$, at 25°C.

3 - Laminated silicon steel

Hysteresis and eddy current losses for silicon steel can be calculated by using well established, classical empirical formulae.

(a) Hysteresis loss

Steinmetz equation predicts hysteresis loss according to

$$P_h = \lambda_h \hat{B}^n f V_e \qquad \text{(W)} \tag{31.48}$$

where λ_h and n are characteristics of the core material:

$n = 1.7$

λ_h = 500 for 4 per cent silicon steel

= 3000 for cast iron

(b) Eddy current loss

Eddy current loss is predicted by

$$P_F = \frac{\left(\pi \hat{B} f t\right)^2}{6\rho} V_e \qquad \text{(W)} \tag{31.49}$$

where t is the thickness of the lamination, parallel to the flux path, and ρ is the magnetic material resistivity. This formula illustrates why high resistivity ferrites have low eddy current loss, even at high frequencies. In the case of iron, the addition of 3-4 per cent silicon increases the resistivity by about four times, reducing both eddy current and hysteresis losses.

Eddy currents produce magnetic fields in the magnetic material, by Lenz's law, which will oppose the applied field. This reduces the flux density in the core centre such that most of the flux is confined to a thin layer or skin near the surface, termed flux *skin effect*.
Within a magnetic material with an ac flux, the flux density cross-section distribution is given by

$$B(x) = B(0)e^{\frac{-x}{\delta}} \qquad \text{(T)} \tag{31.50}$$

where x is the distance from the surface
$\delta = \sqrt{(\rho/\mu_o \pi f)}$ is called the skin depth.

Laminations should be less than ½δ thick. The skin effect in metals can be used to absorb radiated and conducted rfi by using laminations > 2δ thick.

A similar skin effect occurs within conductors carrying ac current, where the current is minimal at the conductor centre. The cross-sectional current density, J, is given by

$$J(x) = J(0)e^{\frac{-x}{\delta}} \qquad \text{(A/m}^3\text{)} \tag{31.51}$$

Below 10-20 kHz and above a few megahertz, solid wire is preferred. In between these frequencies, individually insulated stranded wire, *Litz wire* (after *Litzendraht*) is preferred; decreasing from 0.07 mm to 0.03 mm in strand diameter as the frequency increases and interwinding capacitance dominates.
Copper foil can also be employed.

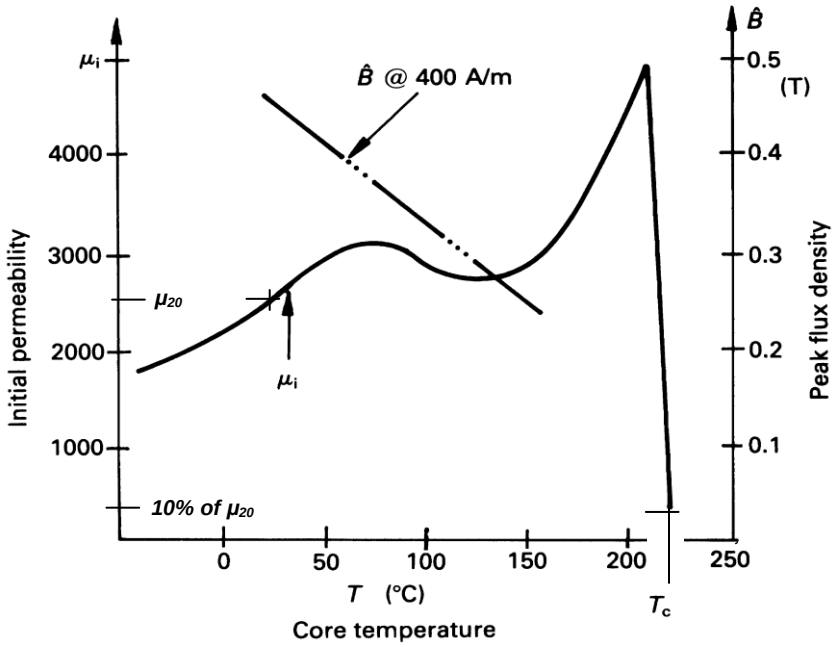

Figure 31.9. *Permeability, μ_i, and maximum density, $\hat{B}$, as a function of core temperature, T.*

31.4.5 Temperature effects on core characteristics

Generally ferrites have poor characteristic temperature stability. At higher temperatures, at the *Curie point*, core materials lose their ferromagnetic magnetic properties abruptly and become paramagnetic ($\mu_e \approx 1$). The temperature causes disruption of the magnet ordering in the crystalline lattice due to molecular thermal motion. The phenomenon is reversible and below the Curie temperature, T_c, the material becomes magnetic again. Typical magnetic material Curie temperatures are:

Fe	770°C
Co	1130°C
Ni	358°C
$Nd_2Fe_{14}B$ (N54)	120°C
Ferrite Mn-Zn	180°C
Nanocrystalline Fe-Si	570°C

The temperature effect on initial permeability in figure 31.9 illustrates the sudden loss of permeability at 212°C, whence the permeability falls to 1, to that of air. The Curie temperature is usually defined as that temperature where the initial permeability falls to 10% of that permeability at 20°C. Generally for ferrites, Curie temperature is inversely proportional to the initial permeability, μ_i. For most ferrites the initial permeability increases with temperature, and reaches a maximum just below the Curie temperature, as shown in figure 31.9.
Other ferrite parameters are also affected by temperature. Increased temperature decreases flux density and hysteresis loss as shown in figures 31.4 and 31.9. The effects of temperature on total core loss per unit volume are shown in figure 31.8a.

31.4.6 Inductance stability

Three factors affect inductance core stability:

- *Parameter effects*
- *Time effects*
- *Temperature effects*

31.4.6i *- Parameter effects*
From the differential of equation (31.22)

$$\frac{dL}{L} = \frac{d\mu_e}{\mu_e} \tag{31.52}$$

while differentiating equation (31.26) yields

$$\frac{d\mu_e}{\mu_e^2} = \frac{d\mu_i}{\mu_i^2} \tag{31.53}$$

Substituting equation (31.53) into equation (31.52) gives

$$\frac{dL}{L} = \frac{L_1 - L_2}{L_1} = \frac{d\mu_i}{\mu_i^2}\frac{A_L}{c} \tag{31.54}$$

The factor $d\mu_i / \mu_i^2$ is constant for a given temperature, hence any change in inductance is due to variations in A_L and c. Thus in order to increase the stability of an inductor in a given material with $\varepsilon << \ell_e$, it is necessary to increase the magnetic circuit air gap (to reduce the inductance factor A_L) or to select a bigger core (to increase the core permeance factor c).

31.4.6ii *- Time effects*
Initial permeability of a ferrite decreases with time under constant operating conditions, including constant temperature. Alternatively, after a ferrite is subjected to shock (thermal, mechanical or magnetic) the permeability increases abruptly, then gradually drifts down over a long period. A *disaccommodation factor*, *df*, independent of effective permeability, is introduced, which characterises the material such that the change in inductance is defined by

$$\frac{dL}{L} = \frac{L_1 - L_2}{L_1} = df\ \mu_e \tag{31.55}$$

The disaccommodation factor is defined by

$$df = \frac{\mu_2 - \mu_1}{\mu_2^2\ \log_{10} t_2/t_1} \qquad \text{for} \quad t_2 > t_1 \tag{31.56}$$

with units of ppm ($/10^{-6}$).
This expression is based on the fact that permeability is proportional to the logarithm of time. The *df* increases slightly with temperature. Generally the *df* decreases, as shown in Table 31.3:

- as the initial permeability increases for a given resistivity
- as resistivity decreases.

The effective disaccommodation factor $df_e = df \times \mu_e$ is the actual disaccommodation of a magnetic circuit where material permeability has been reduced to μ_e by gapping.

Table 31.3: Factors affecting the disaccommodation factor for ferrites

			ρ (Ω cm)		
			10^5	500	≈ 20
μ_i			11-250	800-2000	4000
T_c		°C	450-300	250-170	145
df	$\times 10^{-6}$		50-10	20-2	3

Example 31.1: ***Inductance variation with time***

A pot ferrite core with an effective permeability of 100 ($A_L = 250$) and a disaccommodation factor $df < 35 \times 10^{-6}$ has been in satisfactory operation for five weeks after production. What is the expected inductance variation after 10 years?

Solution

From equation (31.55)

$$\frac{dL}{L} = df\ \mu_e \log_{10}\frac{t_2}{t_1} < 35\times10^{-6}\times100\times\log\frac{520\text{ weeks}}{5\text{ weeks}}$$

that is, dL < 0.7 per cent can be expected.

♣

31.3.6iii *- Temperature effects*

Figure 31.9 shows that between +5°C and +55°C the permeability μ_i variation as a function of temperature is approximately linear for this ferrite. The temperature coefficient of permeability α (or TC) is given by

$$TC = \alpha = \frac{1}{\mu_{i1}}\frac{\mu_{i2}-\mu_{i1}}{T_2-T_1} = \frac{1}{\mu_{i1}}\frac{\Delta\mu_i}{\Delta T} \qquad (\text{K}^{-1}) \qquad (31.57)$$

where $\Delta\mu_i = \mu_{i2} - \mu_{i1}$ is the initial permeability variation over the temperature range $\Delta T = T_2 - T_1$.

The relative temperature factor tf is defined in terms of the temperature coefficient and intrinsic permeability by

$$\alpha_F = \text{temperature factor} = tf = \frac{\alpha}{\mu_{i1}} = \frac{1}{\mu_{i1}^2}\frac{\Delta\mu_i}{\Delta T} \qquad (\text{K}^{-1}) \qquad (31.58)$$

If the permeability variation is large, the temperature factor is modified to

$$\alpha_F = \text{temperature factor} = tf = \frac{1}{\mu_{i1}\mu_{i2}}\frac{\Delta\mu_i}{\Delta T} = \frac{\text{relative temperature coefficient}}{\Delta T} \qquad (\text{K}^{-1}) \qquad (31.59)$$

In a magnetic circuit with an air gap and effective permeability, μ_e, the actual effective temperature coefficient of the core is reduced with gapping according to (see equation (31.42))

$$\alpha_e = \alpha\ \frac{\mu_e}{\mu_i} = \alpha_F\mu_e = tf \times \mu_e \qquad (\text{K}^{-1}) \qquad (31.60)$$

The term $\alpha_F = \alpha_i/\mu_i$ is called the relative temperature coefficient (per unit of permeability). The relative inductance change between two temperatures can be determined by

$$\frac{dL}{L} = \frac{L_2-L_1}{L_1} = \alpha_F\mu_e\Delta T = \frac{\mu_{i1}-\mu_{i2}}{\mu_{i1}\mu_{i2}} \times\ \mu_e \qquad (31.61)$$

For effective permeability μ_e < 80, (that is, a less dominant air gap), the temperature coefficient $\alpha_e = \mu_e\alpha_F$ should be increased by 10 to 30 × 10^6/K to account for the temperature influence of the winding.

Example 31.2: ***Temperature effect on inductance***

The gapped pot core in example 31.1 is specified by a relative temperature coefficient of 1 x 10^6/K. What is the expected inductance variation over the temperature range 25 to 55°C?

Solution

From example 31.1

$$\mu_e = \frac{A_L}{c} = \frac{250}{2.5} = 100$$

$$\Delta T = 55 - 25 = 30°\text{C}$$

From equation (31.61)

$$\frac{dL}{L} = \alpha_F \mu_e \Delta T$$
$$= 1 \times 10^{-6} \times 100 \times 30 = 0.3 \text{ per cent inductance variation}$$

♣

Whilst permeability decreasing with ageing for ferrite, and significantly so for Cobalt based amorphous metals, nanocrystalline and non-alloyed metals are comparatively stable.

31.4.7 Stored energy in inductors

The energy stored in the magnetic field in the core (before saturation) is given by

$$E = \tfrac{1}{2} BH \check{V}_e \qquad \text{(J)} \tag{31.62}$$

where $\check{V}_e$ is the effective minimum core volume. It can be shown that before saturation, the stored magnetic energy is equivalent to the stored electrical energy, whence

$$E = \tfrac{1}{2} BH \check{V}_e = \tfrac{1}{2} Li^2 \qquad \text{(J)} \tag{31.63}$$

For un-gapped cores, like a toroid, the ferrite effective volume, V_e, is equal to the minimum effective volume, $\check{V}_e$. Inductors meeting this requirement may necessitate an excessive core size. However the introduction of an air gap, ε, can reduce the core size significantly, since a significant amount of the energy can be stored in the gap volume. The minimum effective volume is now larger than the ferrite core effective volume, and is given by

$$\begin{aligned} \check{V}_e &= V_e + A_e \mu_i \varepsilon \\ &= A_e \left(\ell_e + \mu_i \varepsilon \right) \qquad (\text{m}^3) \end{aligned} \tag{31.64}$$

Figure 31.10 shows modified *B*-*H* characteristics (no hysteresis) for air gap inductors. The line curve o-b represents the core without an air gap, which results in the largest inductance. The energy stored in the core for a flux BA_e, in the linear portion of the curve, is the area of the shaded triangle 0-a-b, as defined by equation (31.62). When an air gap is introduced, the effective permeability falls as shown by the decreased slope of line o-c. The figure shows that as the air gap increases, the inductance decreases. It can be shown that the stored energy in the air gap and core is represented by the shaded area o-a-c, for a given flux, BA_e. It can be seen that the energy stored in the gap of length ε, o-b-c, although its length is much shorter than the core length, ℓ_c, is much greater than that stored in the core, 0-a-b.

The total energy stored o-a-c, E_T, in the magnetic circuit comprises the energy stored in the air gap, o-b-c, E_ε, plus the energy stored in the magnetic core material, o-a-b, E_{core}. These two energies are equal to the areas of the shaded triangles, o-b-c and o-a-b, respectively in figure 31.10. That is

$$\begin{aligned} E_T &= E_{core} + E_\varepsilon \\ &= \tfrac{1}{2} B_c H_c V_c + \tfrac{1}{2} B_\varepsilon H_\varepsilon V_\varepsilon \end{aligned} \tag{31.65}$$

If leakage is neglected, then the air gap flux is the same as the core flux. If fringing is neglected then the area of the core at the air gap is the same as the area of the gap. Then

$$\begin{aligned} E_T &= \tfrac{1}{2} BH_c A_e \ell_c + \tfrac{1}{2} BH_\varepsilon A_e \varepsilon \\ &= \tfrac{1}{2} BA_e \left(H_c \ell_c + H_\varepsilon \varepsilon \right) \end{aligned} \tag{31.66}$$

For a gapped core, as shown in figure 31.13, from Ampere's current law (horizontal axis in figure 31.10)

$$Ni = H_c \ell_c + H_\varepsilon \varepsilon \tag{31.67}$$

Therefore, substituting equation (31.67) into equation (31.66) gives the total stored energy as

$$\begin{aligned} E_T &= \tfrac{1}{2} BA_e \left(H_c \ell_c + H_\varepsilon \varepsilon \right) \\ &= \tfrac{1}{2} BA_e \left(Ni \right) = \tfrac{1}{2} \phi Ni \end{aligned} \tag{31.68}$$

which is equal to the area of the shaded triangle o-a-c.

The inductance *L* is given by equation (31.4), that is

$$L = \frac{N\phi}{i} \tag{31.69}$$

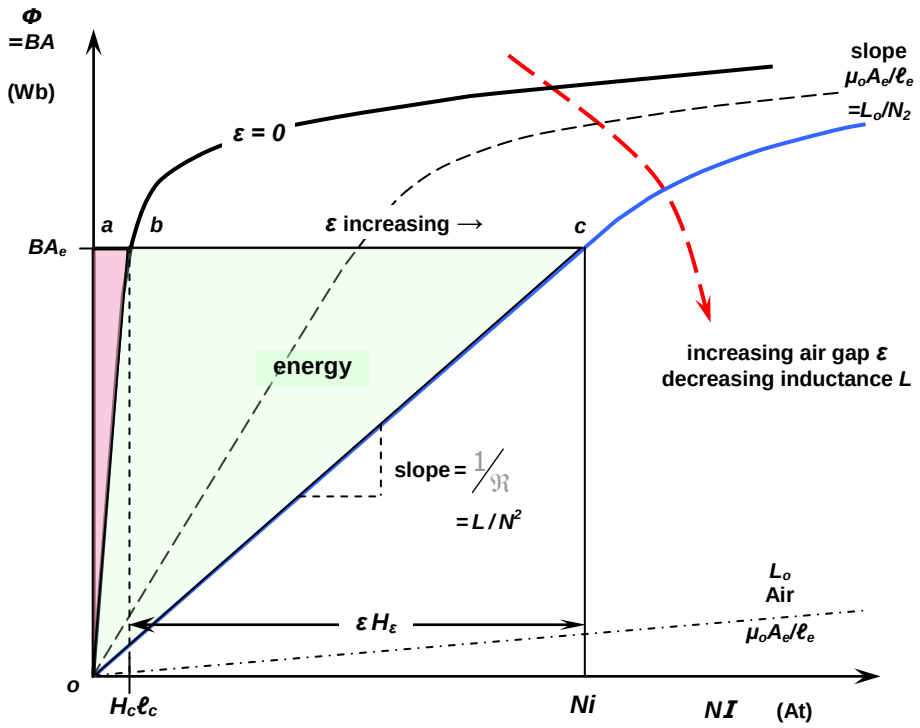

Figure 31.10. *Effects of an air gap on inductance and stored energy.*

Substitution of equation (31.67) for the current *i* gives

$$L = \frac{N^2\phi}{H_c\ell_c + H_\varepsilon\,\varepsilon} = \frac{N^2 A_e\mu_o}{\frac{\ell_c}{\mu_r}+\varepsilon} = \frac{N^2 A_e\mu_o}{\ell_c+\varepsilon}\left[\frac{(\ell_c+\varepsilon)\mu_r}{\ell_c+\mu_r\,\varepsilon}\right] = \frac{N^2 A_e\mu_o\mu_e}{\ell_{total}} = \frac{N^2}{\Re} \qquad (31.70)$$

where $\ell_{total} = \ell_c + \varepsilon$ and

$$\mu_e = \frac{(\ell_c+\varepsilon)\mu_r}{\ell_c+\mu_r\,\varepsilon} \qquad (31.71)$$

Making the usual assumption that the length of the core is much greater than the length of the air gap, $\ell_c >> \varepsilon$, yields equation (31.28) for the effective permeability.

31.5 Ferrite inductor and choke design, when carrying dc current

Air gaps in magnetic circuits are introduced in order to reduce the influence of a superimposed dc current, manufacturing dispersion and/or to improve parameter stability. Saturable inductors for a semiconductor switch turn-on snubber normally do not employ an air gap, in order to reduce the stored energy, which may be subsequently dissipated, and to minimise the magnetising current magnitude.
Empirical equations have been derived for cylindrical inductors with a cylindrical core, which give an inductor with a large air gap. Design equations and examples are given in Appendix 31.11.

31.5.1 Linear inductors and chokes

The introduction of an air gap reduces the effective permeability, μ_e such that the coil inductance is given by the equation (31.22)

$$L = \mu_e c N^2 = \mu_e L_o = A_L N^2 \qquad \text{(H)} \qquad (31.72)$$

Figure 31.11a shows the variation of the effective permeability, μ_e at both low flux levels and without a dc bias, as a function of the relative air gap, ε/ℓ_e as specified by equation (31.27). As the air gap and the superimposed dc field are varied, the incremental permeability, μ_Δ varies as shown in figure 31.11b. This figure indicates how inductance varies with dc bias current (*H*).

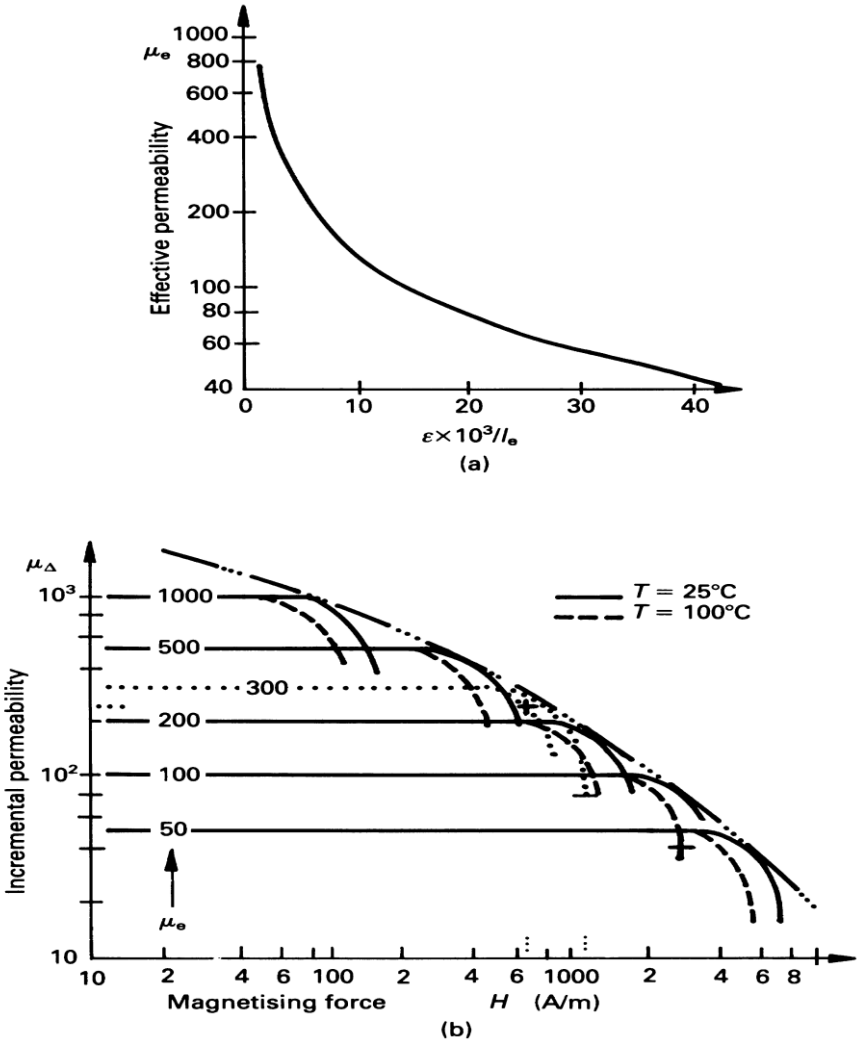

Figure 31.11. *Permeability as a function of: (a) air gap, ε and (b) superimposed dc field and air gap.*

Figure 31.11 does not specify the optimum inductor design since for a given inductance and dc current the optimum air gap and number of turns are not specified. The minimum number of turns and air gap requirements, for a dc current, can be determined by means of the Hanna curves in figure 31.12.

This figure shows an experimental family of curves of per unit core energy against magnetomotive force per unit length, for different air gap widths. The resultant curves are ferrite type dependent and dimensionally independent. Hanna curves therefore allow the determination of minimum turns N and air gap ε, from the required inductance L and dc current I.

Three distinct energy levels are shown in the Hanna curves in figure 31.12.

i. At low dc currents (H) the per unit energy increases linearly with H. This region corresponds to the horizontal regions in figure 31.11b, where

$$L = \mu_\Delta c N^2 \quad \text{(H)} \tag{31.73}$$

and as H varies, μ_Δ is constant.

ii In the mid energy region, the per unit energy can decrease with increased H. The incremental permeability decreases, causing L to decrease at a greater rate than the increase in the dc current squared, I^2. This region is characterised by the fall off in μ_Δ, hence inductance, as H increases as shown in figure 31.11b.

iii. At high dc currents, the core material saturates, and μ_Δ tends to unity. Air core inductance results, where

$$L = L_o = c N^2 \tag{31.74}$$

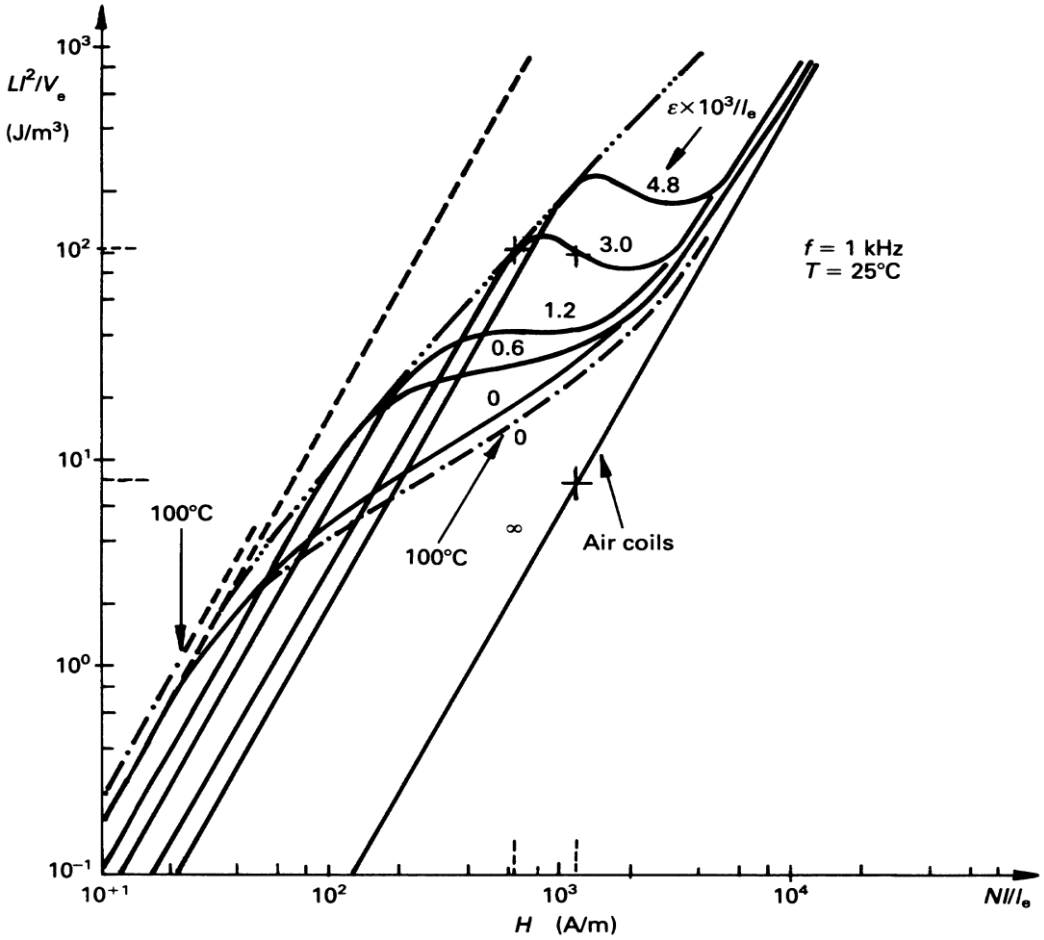

Figure 31.12. *Hanna curves, showing trajectories for different air gaps.*

Example 31.3: ***Inductor design (ferrite) with Hanna curves***

A 20μH, 10A choke is required for a forward converter. The inductance must be constant for unidirectional currents to 10 A. An available E-core pair has the following effective parameters

$\ell_e = 0.11$ m, $A_e = 175 \times 10^{-6}$ m^2, $V_e = 19.3 \times 10^{-6}$ m^3 and
$\mu_i = 2500$ @ 25°C and 3000 @ 100°C (from figure 31.9)

i. At a core temperature of 25°C, determine the required air gap and turns. Allow a 5 per cent decrease in inductance at rated conditions.
ii. Estimate the inductance at 20A dc.
iii. Calculate the inductance at 10A and 20A dc, both at 100°C.

Solution

i. Evaluate $\dfrac{LI^2}{V_e} = \dfrac{20 \times 10^{-6} \times 10^2}{19.3 \times 10^{-6}} = 104$ J/m^3

From figure 31.12, restricted to the constant-*L* region, 104 J/m^3 corresponds to
(a) $\varepsilon/\ell_e = 3 \times 10^{-3}$
whence $\varepsilon = 3 \times 10^{-3} \times \ell_e = 3 \times 10^{-3} \times 0.11$
The required total air gap is 0.33 mm
(b) $H = 650$A/m
Since $H = NI/\ell_e$
$N = H\ell_e/I = 650 \times 0.11/10 = 7.15$ turns
Use 7 turns and a 0.33 mm total air gap.

ii. At 20 A, 25°C
$H = NI/\ell_e = 7 \times 20/0.11 = 1270$A/m
Two alternative design approaches may be used to estimate the inductance.

(a) The effective permeability, μ_e, before saturation can be evaluated from equation (31.27)

$$\frac{1}{\mu_e} = \frac{1}{\mu_a} + \frac{\varepsilon}{l_e} = \frac{1}{2500} + 3 \times 10^{-3}$$

that is

$$\mu_e \approx 300$$

From figure 31.11b, for μ_e = 300 it can be seen that the incremental permeability μ_Δ is constant, as required to 650A/m, then μ_Δ decreases as saturation commences. At H = 1270A/m, μ_Δ has fallen to 75, from 300. The incremental inductance at 20 A is about ¼ of 20μH, namely 5.0μH.
(b) Alternatively, a simpler approach uses only figure 31.12. H = 1270A/m projects 100 J/m^3. Solving 100.0 = $L_{20A} I^2 / V_e$ with I = 20A yields L_{20A} = 5μH.

iii. The effective permeability at 100°C is

$$\frac{1}{\mu_e} = \frac{1}{\mu_i} + \frac{\varepsilon}{l_e} = \frac{1}{3000} + 3 \times 10^{-3}$$

that is

$$\mu_e \approx 300$$

It is seen that, although the initial permeability varies significantly with temperature, here the effective permeability is dominated by the air gap, hence is essentially temperature independent. Figure 31.11b, with H = 640A/m, projects μ_Δ = 220 at 100°C. Using $L \propto \mu_\Delta$, the inductance falls to about 15μH at 100°C, 10 A.
At 20A, 100°C, the effects of saturation are highly significant, and figure 31.11b indicates that the incremental permeability is low. The best approximation is to use the air coil curve in figure 31.12. Hence H = 1270A/m projects 9J/m^3. From 9 = $L_{20A} I^2 / V_e$, at 20A, 100°C, an inductance of at least 0.43μH can be expected.

♣

Figure 31.5 shows how μ_Δ and hence the inductance, falls off as H, and hence the current, increases for ferrite core materials. The larger the air gap, and hence the lower A_L and the lower L, the higher H before inductance rolls off. Inductance rolls off faster, the wider the air gap, hence the higher the magnetic field strength, H. The decrease in effective permeability, μ_e and inductance factor, A_L, with increase of air gap, ε, is shown in figure 31.13 for two E-cores.

Figure 31.14 shows typical curves for the decrease in μ_Δ, hence inductance, with increased H, hence current, for both ferrites and alloy or iron powder cores. Because power ferrites have a squarer B-H curve than powder cores, the inductance of ferrites falls off faster. By increasing the core volume, the fall off rate of inductance can be reduced. Depending on core loss for a given volume, a powder core may be more effective than a ferrite; and would have better utilisation of the copper window area. The design approach previously considered in example 31.3 in fact neglects the optimisation of core size and copper I^2R loss.

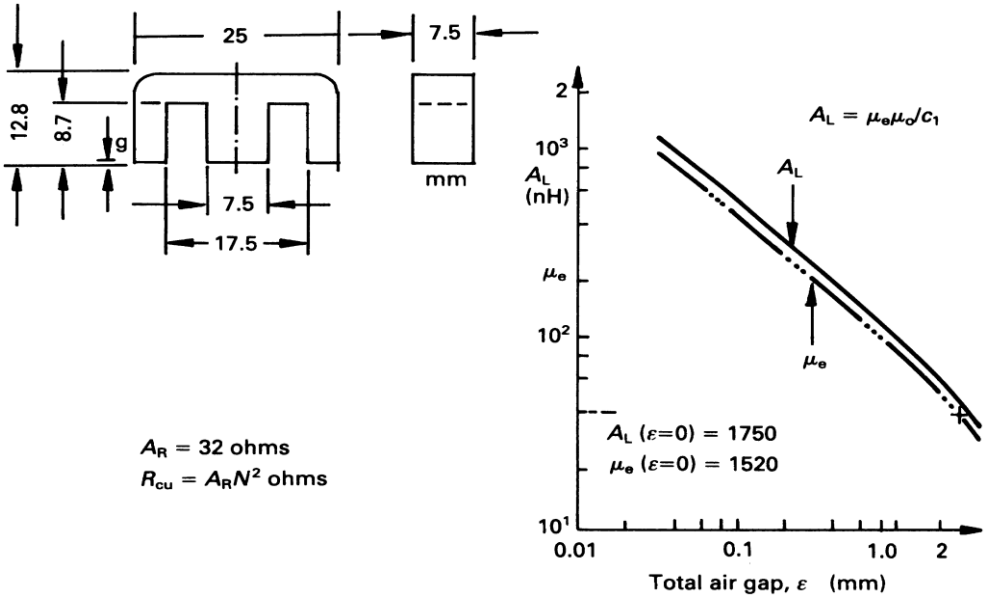

Figure 31.13. *Characteristics of a pair of gapped E-cores. Core dimensional parameters are given in table 31.5.*

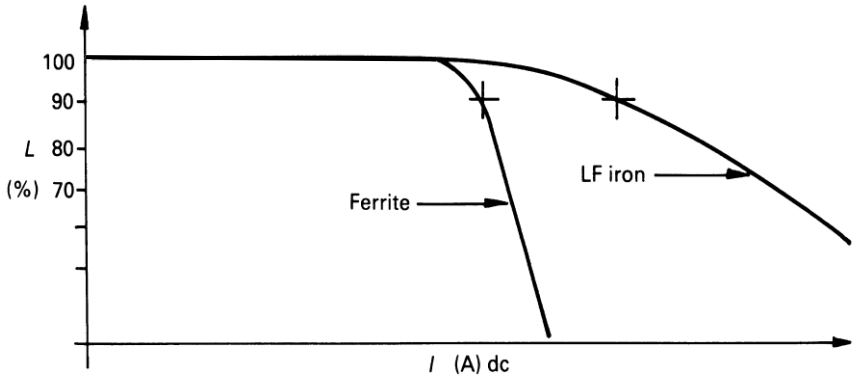

Figure 31.14. *Comparison of inductance characteristics illustrating how inductance falls off faster with ferrite cores than with iron cores, at higher currents.*

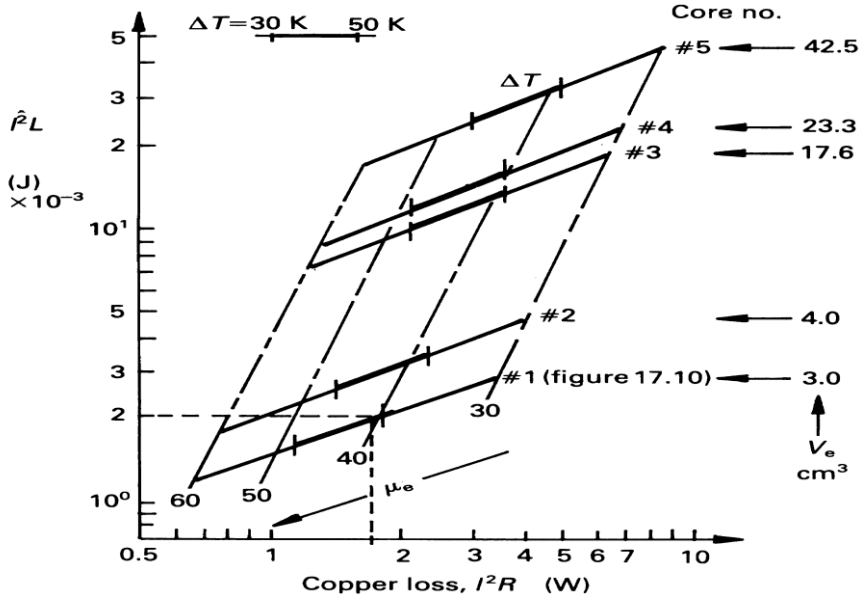

Figure 31.15. *Magnetic biasing capability $\hat{I}^2L$, copper loss I^2R, effective permeability μ_e and over-temperature ΔT of five different effective volume V_e ferrite cores.*

31.5.1i - Core temperature and size considerations

Figure 31.15 relates stored energy, LI^2, and copper loss, I^2R, for different cores of the same ferrite type. Once L and I are fixed, figure 31.15 can be used to determine the optimum core size and air gap. This figure shows that with increasing air gap (decreasing μ_e), the magnetic biasing capability increases along with the associated copper loss, I^2R. A flowchart is shown in figure 31.16, which outlines the inductor iterative design procedure to be used in conjunction with figure 31.15.

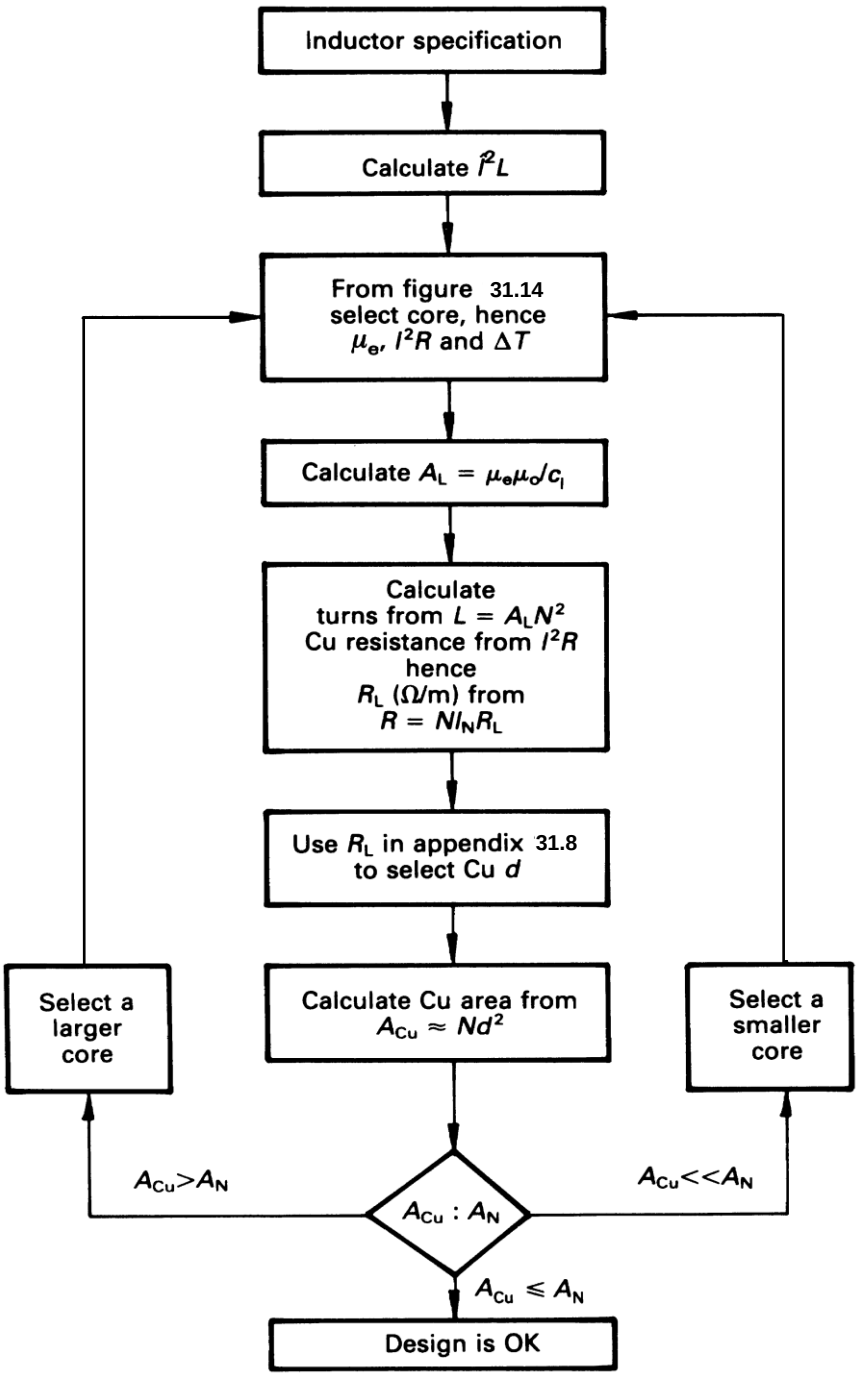

Figure 31.16. *Linear inductor design flowchart.*

Example 31.4: ***Inductor design including copper loss***

With the aid of figure 31.15, design a 20μH, 10A dc inductor, calculating the copper loss and temperature rise for the predicted optimum air gap and number of turns.

Solution

Following the procedure outline in the flowchart of figure 31.16:

Evaluating $LI^2 = 20 \times 10^{-6} \times 10^2 = 2$ mJ

From the monogram in figure 31.15 use core # 1, with $\mu_e = 40$ and $I^2R = 1.8$ W. This copper loss will produce a 50°C temperature rise above ambient on the core surface, beneath the winding. The thick bars in figure 31.15 represent a 30 to 50°C temperature increase range.

The core type # 1 has A_L and μ_e values versus total air gap, and effective parameters as shown in figure 31.13 and Table 31.5. For $\mu_e = 40$, $A_L = 45$ nH, a total air gap of 2.7 mm is required.

From $L = A_L N^2$

$$N = \sqrt{20 \times 10^3/45} = 21 \text{ turns}$$

For $I = 10$ A dc, $I^2R_{Cu} = 1.8$ W, then $R_{Cu} = 18$ mΩ. The copper turns diameter is determined from

$$R_{Cu} = N\ \ell_N\ R_L \quad (\Omega) \tag{31.75}$$

where R_L is the resistance per metre, Ω/m.

ℓ_N is the mean turn length which is either provided for a given former or may be estimated from core physical dimensions. From Table 31.5:

$\ell_N = 52$ mm

$R_L = R_{Cu} / N\ell_N$

$= 18 \times 10^{-3}/21 \times 52 \times 10^{-3} = 0.165$ Ω/m

Using standard wire tables, Appendix 31.12 for 0.165 Ω/m, use 28 SWG (0.154 Ω/m) which has a diameter of 0.36 mm and 0.434 when enamelled. The resultant copper current density is 77 A/mm^2.

In many applications 4 A/mm^2 is used for finer gauge wires up to 20 A/mm^2 for heavier gauge wires. These current densities represent about 5 per cent of the fusing current, I_{fusing} which is approximated by

$$I_{\text{fusing}} = 80\,d^{1.5}$$

The diameter d is in mm.

This constraint is unrealistic and inductor and transformer design is based on temperature rise.

The approximate copper area is

$$A_{Cu} = N \times d^2$$
$$= 21 \times 0.434^2$$
$$= 3.88\text{mm}^2$$

From Table 31.5, the useful winding cross-section is

$$A_N = 56 \text{ mm}^2$$

Only 8 per cent of the former window area is filled, hence the actual copper length is overestimated and I^2R loss, hence temperature rise, will be less than the allowed 1.8 W and 50°C respectively.

♣

Comparing the design of examples 31.3 and 31.4, it will be seen that the same design specification can be fulfilled with the latter core of 20 per cent the volume of the former. The bigger core required an 0.33 mm air gap to give $\mu_e = 300$, while the smaller core required a larger gap of 2.7 mm to give $\mu_e = 40$. Both cores are of the same ferrite type. The incremental inductance of the smaller core will fall off with current, much faster than with the larger core, as indicated by figure 31.5.

For a switch mode power supply application, the rms value of current is less than the peak current at which the inductance is specified. The copper loss, hence temperature rise, is then based on an rms current basis.

Inductor design constraints

The inductor design procedure outline and example fulfil a basic underlying energy per unit volume constraint. An inductor specification involves designing an inductor of L Henry, capable of carrying an rms current of I_{rms} and peak current of I_p.

If the wire area is a_w m^2 and has a maximum safe operating current density of J, then

$$a_w = \frac{I_{rms}}{J}$$

If the peak flux density B_{max} in the core of effective area A_e is produced by peak current I_p in the inductor winding:

$$LI_p = N\phi_p = NA_eB_{\max}$$

The inductor winding of N turns is accommodated in the core window and the window area A_N is filled by the conductors with a packing fraction k_w, then

$$k_w A_N = Na_w = N\frac{I_{rms}}{J}$$

Combining these equations

$$LI_pI_{rms} = k_w JB_{\max} A_e A_N$$

This equation may be interpreted as a relationship between the energy handling capacity $\frac{1}{2}LI^2$ of the inductor to the size of the core A_eA_N, and the material properties B_{max}, J and construction constraints k_w.

31.5.2 Saturable inductors

Saturable inductors are used in series with semiconductor switching devices in order to delay the rise of current, thereby reducing switch turn-on stress and loss. In the case of a power transistor, the collector current is delayed until the collector voltage has fallen (see 9.3.4). For thyristor devices, the delay time allows the gate activated cathode area to spread hence giving a high initial *di/dt* capability. In each case the inductor supports the supply voltage, then after a finite time saturates to a low inductance, supporting little voltage, and does not influence the switch current.
Ferrites are ideal as the core of a saturable inductor because of their low magnetic field strength, H_s, at the onset of flux density saturation, B_s. While the inductor supports voltage, v, the flux density increases, moving up the *B-H* curve at a rate according to Faraday's law

$$v = NA_e \frac{dB}{dt} \tag{31.76}$$

A low magnetising current results. After a finite time the flux density reaches the knee of the *B-H* curve (B_s, H_s), the core saturates and the incremental permeability falls from an initially high value to that of air, $\mu_\Delta = 1$. The high initial permeability, hence high inductance, limits the initial current. The time t_s, for the core to saturate should be equal to the switch turn-on voltage fall time, t_{fv}. The low saturation inductance allows the switch current to rapidly build up to a level dictated by the load.
If the switch voltage fall is assumed linear then the inductor voltage rise is $V_s\, t / t_{fv}$. The time t_s, taken to reach core saturation (B_s, H_s) from integration of Faraday's law is (see Chapter 9.3.4)

$$t_s = \frac{2NA_eB_s}{V_s} \tag{31.77}$$

for $t_s \le t_{fv}$.
The flux density, hence H, and current increase quadratically with time, $I_s\left(t / t_{fv}\right)^2$. At saturation the magnetising current magnitude (hence switch current) is

$$I_s = \frac{H_s \ell_e}{N} \quad \left(= \frac{2B_sH_sV_e}{t_sV_s}\right) \qquad \text{(A)} \tag{31.78}$$

which should be small compared with the switch on-state full-load current magnitude.

The inductance before saturation is given by

$$L = A_L N^2 \qquad \text{(H)} \tag{31.79}$$

and falls to that of an air-cored inductor, viz.:

$$L_{sat} = c\,N^2 \qquad \text{(H)} \tag{31.80}$$

after saturation, when leakage and lead length will, in practice, dominate inductance.

The energy stored in the core (pre-saturation) and subsequently dissipated at core reset is given by

$$\begin{aligned} E &= \tfrac{1}{2}B_sH_sV_e \quad \left(= \tfrac{1}{4}I_sV_st_s\right) \\ &= \tfrac{1}{2}B_sH_sA_e\ell_e \qquad \text{(J)} \end{aligned} \tag{31.81}$$

which must be minimised.

Table 31.4 summarises saturable inductor requirements based on equations (31.77) to (31.81).

Table 31.4: Design requirement of a saturable inductor

Given V_S and t_{fv}		Material dependent		Core shape dependent		
		H_s	B_s	A_e	ℓ_e	N
Minimise energy $E = \tfrac{1}{2}\, B_s H_s A_e \ell_e$	E (J)	low	low	low	low	×
Maximise time $t_s = 2NA_eB_s / V_s$	t_s (s)	×	high	high	×	high
Minimise mag current $I_s = H_s \ell_e / N$	I_s (A)	low	×	×	low	high
Maximise inductance $L_a = N^2 A_e B_s / \ell_e H_s$	L (H)	low	high	high	low	high
Requirement		low H_s (high μ_r)	-	-	short ℓ_e	high N
Compromise		-	high B_s if H_s is low	high A_e if ℓ_e is short		

31.5.3 Saturable inductor design

Figure 31.17 shows a saturable inductor iterative design flowchart. The design starting point is the type of ferrite. The desired ferrite should have minimal high frequency loss, associated with a low magnetic field intensity, H_s, at saturation. These features would be associated with ferrites having a low coercive force, H_c and remanence, B_r. The ferrite material shown in figure 31.4 fulfils these requirements with

$$H_c = 12\text{A/m} \qquad B_r = 0.18\text{T}$$
$$H_s = 200\text{A/m} \qquad B_s = 0.4\text{T}$$

Ferrites with lower magnetic field strengths are available but tend to be limited in size. A material with a high initial permeability is one indicator of a suitable ferrite type.

The next considerations are core shape and effective core parameters such as effective length, ℓ_e and area, A_e. The core should have a short effective length, ℓ_e. The area and length are traded in maintaining sufficient copper window area, A_N.

A core shape without an air gap will produce the highest possible initial, hence effective, permeability. Example 31.5, which follows, illustrates that a toroid (or tube) core offers a good solution. The preferred ferrite material for saturable rectors is type 3R1 or an equivalent.

A high number of turns, N, is desirable, and preferred to an increase in area, A_e.

Design should be based on the maximum core temperature. An increase in temperature decreases H_s at a faster rate than B_s, as shown in figure 31.4. From equation (31.77), many turns are required which, in combination with decreased H_s, advantageously decrease the magnetising current, I_s.

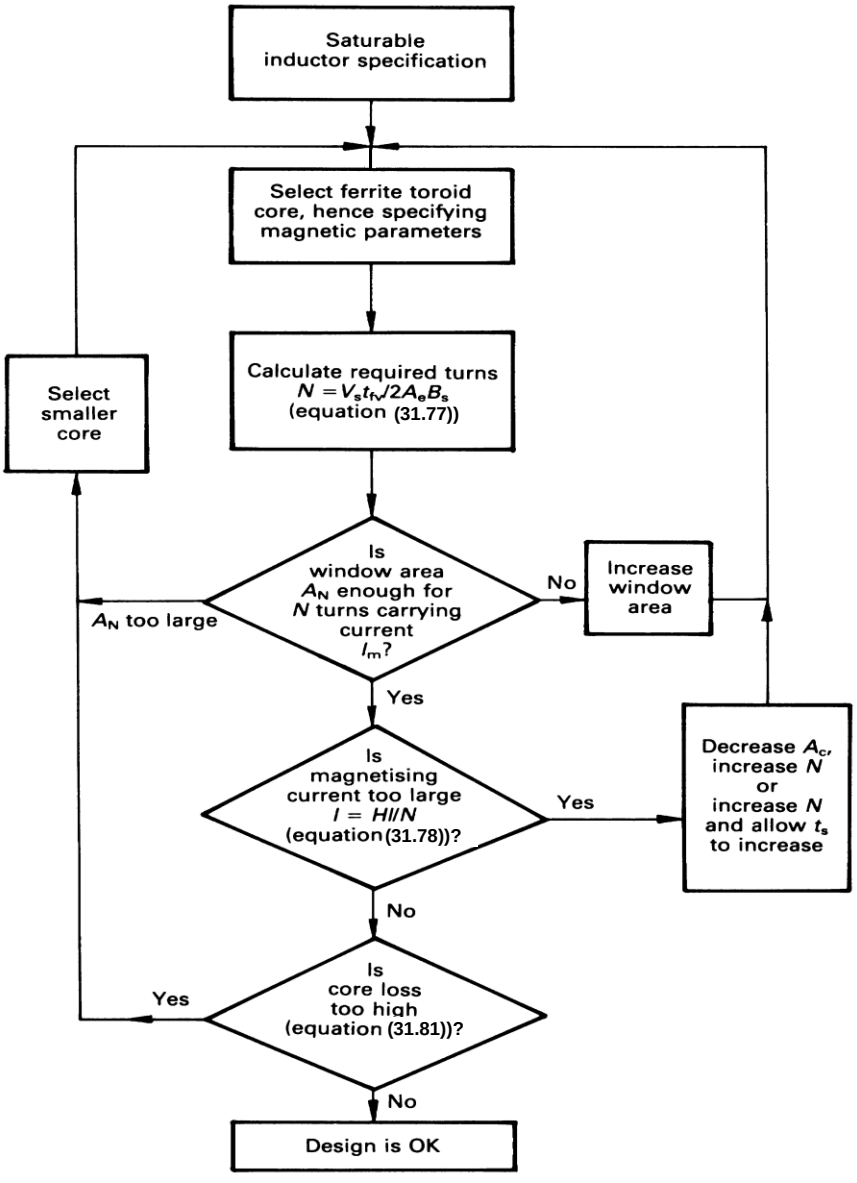

Figure 31.17. *Saturable inductor design flowchart.*

Table 31.5: Pot, toroid, and E-core design data.
Applicable magnetic data are presented in Appendix 31.8

		Physical dimensions (mm)		
		Pot core d_o = 25 h = 16	Toroid d_o = 39 d_i = 24.77 h = 6.61	E-core (pair) see figure 31.13
V_e	cm^3	3.63	3.86	3.02
A_e	cm^2	0.999	0.398	0.525
ℓ_e	cm	3.64	9.71	5.75
c_1	cm^1	3.64	24.4	10.9
A_{min}	cm^2	0.95	0.398	0.45
A_L	nH	4300	1540	(ε = 0)1750
μ_e		1245	(μ_i) 3000	(ε = 0)1500
c	nH	3.45	0.51	1.15
A_N	cm^2	0.357 (0.266)	4.75	0.56
ℓ_N	cm	5.3 (5.35)	7.6	5.2
S_A	cm^2	18.4	48.7/58	20
weight	g	23.4	19.3	2 × 8

Example 31.5: ***Saturable inductor design*** (also see example 8.6)

A pot, toroid, and E-shaped core of the same Mn-Zn ferrite as characterised in Appendix 31.8, and of similar volume, have characteristics and parameters as shown in Table 31.5, with H_s = 200At/m.
Design a saturable inductor for each core shape, for a switch having a 200ns linear voltage fall time at turn-on when switching on a V_s = 600 V dc supply rail.
The core is to saturate when the switch voltage reaches saturation (0 V), after 200ns.
Estimate the core power removed at reset if the switching frequency is 20 kHz.

Solution

	Pot	Toroid	E-cores (ε = 0)
From equation (31.77) $N = V_s t_{fv} / 2A_e B_s = 1.875 / A_e$ A_e is in cm^2	2	5	4
From equation (31.78) $I_s = H_s \ell_e / N = 2\ell_e / N$ (A) ℓ_e is in cm	3.64	3.85	2.83
From equation (31.79) $L = A_L N^2 \times 10^{-3}$ (μH)	20.2	38.5	28.0
From equation (31.80) $L_{sat} = c N^2$ (nH)	13.8	12.75	18.4
From equation (31.81) $P_d = V_e \times 8{\times}10^{-1}$ (W) V_e is in cm^3	2.90	3.09	2.42

Based on the available copper window area, A_N and number of turns, the cores would be applicable to switching currents in excess of 100 A. Smaller cores could be used for lower current levels, although window area A_N tends to dictate the required core.
From equation (31.81), the power dissipated at 20 kHz (last row in the table) is given by $P_d = ½B_s H_s V_e f_s$.

♣

31.6 Power ferrite transformer design

Above a few kilohertz, Mn-Zn ferrite material is almost exclusively used for power transformer cores, and has been optimised by manufacturers for a wide frequency range. Specific core shapes have also been developed to cover a wide power range. In the case of voltage transformers, at 20kHz and below 100W, pot cores are used, or when low flux leakage and low emi are important. Such cores can be processed on automatic machines which wind and assemble the whole unit. At powers above 100 W, E-E and E-I cores are extensively used.
The usable power range of the pot core is increased by increasing frequency and at 500 kHz no alternative exists, because of the low leakage flux, low self-capacitance, and good shielding offered by pot cores.

31.6.1 Ferrite voltage transformer design

To simplify ferrite core selection, manufacturers provide the characteristic curves given in figure 31.18 which show the power that can be transmitted by various core shapes. Specifically, these curves show power for the modes of operation commonly used in switch-mode power supplies; such as push-pull, forward, and flyback, as considered in chapter 19, versus the core plus copper volume.
A formal transformer design approach based on copper and core losses is shown in the flowchart in figure 31.19 and is applicable to all smps types.

Stage 1 and stage 2

The transformer, primary and secondary voltages, currents, and powers, hence efficiency, must be specified or determined. Other requirements are switching frequency, ambient temperature, and allowable temperature rise at the core to copper interface. The final specification should include

$$\begin{matrix} V_p & V_s \\ I_p & I_s \\ P & P \end{matrix} \qquad \eta, f, T_a, \Delta T$$

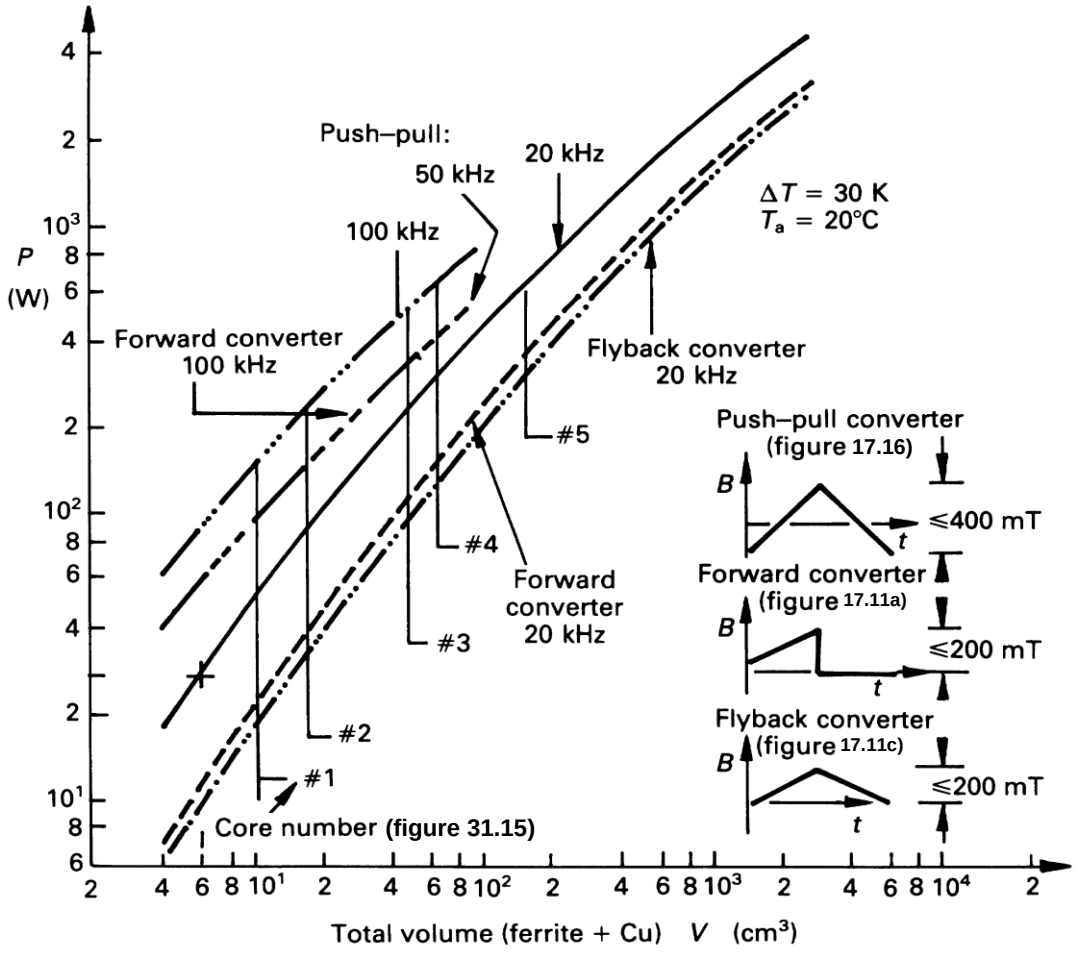

Figure 31.18. *Transmissible power, P, versus volume (ferrite plus copper), V, of transformers with ferrite Mn-Zn cores.*

Stage 3

The difference between input power and output power is the total power loss, P_L, which comprises copper and core losses. The maximum efficiency is obtained when the copper loss equals the core loss.

Stage 4

The total power loss, P_L, ambient temperature, T_a, and temperature rise, ΔT, specify the exposed copper and core surface area requirements, S_A, according to (see equation 5.4)

$$S_A = \frac{P_L}{\Delta T\, S_d} \quad (\text{m}^2) \tag{31.82}$$

where S_d is a surface dissipation factor.

Empirical equations are commonly provided for S_d. Based on the assumption that thermal stability is reached half by convection and half by radiation, the surface area requirement can be approximated by

$$S_A = 145 \times \left[\frac{1000}{T_a + 273}\right]^{2.06} \frac{P_L}{\Delta T^{1.22}} \quad (\text{cm}^2) \tag{31.83}$$

Stage 5

A core with the minimum surface area, S_A, is selected using manufacturers' data, ensuring that the ferrite type is appropriate to the operating frequency and that the core shape meets any engineering, cost or other special requirements. The manufacturers' data required include the effective dimensional parameters, copper winding area, A_N, and average turn length, ℓ_N.
Some manufacturers provide transformer design data for each core. This specific data can be employed, rather than the general procedure that follows.

Stage 6

Using the core volume, V_e, and core loss $P_c = ½P_L$, whence core loss per cm^3, $P_w = P_c / V_e$ the maximum allowable operating flux density, B_{op}, for the specified frequency can be determined from the power loss curves in figure 31.8c.

Stage 7

The rated saturation flux density, B_s, cannot safely be used. For a transformer using both quadrants of the *B-H* characteristics, for example, a push-pull smps transformer

$$B_{op} \le 0.8 B_s$$

while for a core used with a flux bias

$$B_{op} \le 0.4 B_s$$

These limits avoid operational saturation of the core in one direction. If the working flux density, B_{op}, is too high, either

- reduce the efficiency and go to stage 1/2, or
- reduce the allowable temperature rise and go to stage 4.

Stage 8

The required number of primary turns, N_p, can be calculated from Faraday's law, which yields

$$N_p = \frac{V_p}{k\, B_{op} A_e f} \tag{31.84}$$

where $k = 4$ for a square-wave voltage
$k = 4.44$ for a sine wave.
If $B_{op} > 100$ mT, the effective area, A_e, in equation (31.84) is replaced by the core minimum area section, A_{min}, since that portion experiences the highest flux density.

The number of secondary turns is calculated according to

$$N_s = N_p \frac{V_s}{V_p} \tag{31.85}$$

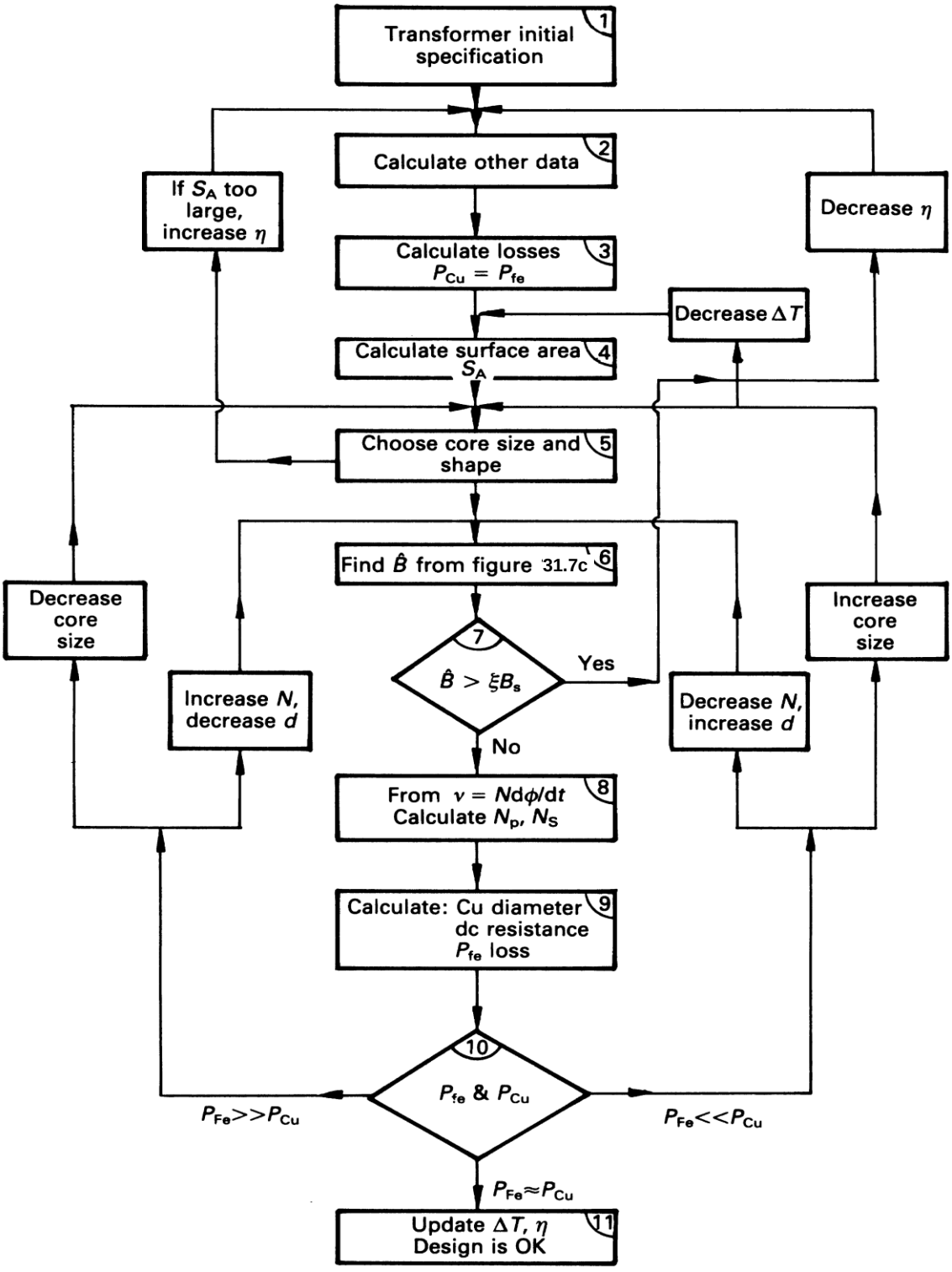

Figure 31.19. *Voltage transformer design flowchart.*

Stage 9

The winding diameter, d_p, for the allotted primary for a window area, A_p, is calculated according to

$$d_p = 2\sqrt{\frac{A_p k_w}{\pi N_p}} \quad \text{(m)} \tag{31.86}$$

where k_w is a winding space factor, 0.7, which accounts for insulation, winding taps, shielding, air space, etc. A similar expression for the diameter of the secondary, d_s, involves the number of secondary turns, N_s, and allotted area, A_N. The total winding area $A_p + A_s$ must not exceed the available winding area, A_N.

Standard copper wire tables, Appendix 31.12, provide the resistance per metre, R_L, for the calculated diameters. From equation (31.75), the dc resistance of the primary can be calculated according to

$$R_p = N_p \ell_N R_{Lp} \quad (\Omega) \tag{31.87}$$

Similarly for calculating the secondary dc resistance, R_s. The total copper loss can be calculated as

$$P_{Cu} = I_p^2 R_p + I_s^2 R_s \quad (\text{W}) \tag{31.88}$$

Stage 10

The core loss, P_c, and the copper loss, P_{Cu} are compared. If

(i) $P_{Cu} > P_c$

Either decrease the number of turns and increase the copper diameter. This will reduce the copper loss and increase B_{op}, and hence P_c. Recalculate from stage 6.

or select a larger core, which will increase the copper window area, A_N, hence increasing the allowable wire diameter. Recalculate from stage 5.

(ii) $P_{Cu} < P_c$

Either increase the number of turns which will reduce diameter d, B_{op} hence P_c, and then recalculate from stage 6.

or select a smaller core, which will require d to be reduced, and then recalculate from stage 5.

Proceed if $P_{Cu} \approx P_c$.

Stage 11

Update the value of total losses, P_L, and hence recalculate the power requirements and resultant efficiency.

Calculate the actual core temperature rise from equation (31.83), rearranged

$$\Delta T = 59\left(\frac{1000}{T_a + 273}\right)^{1.69} \times \left(\frac{P_L}{S_A}\right)^{0.82} \quad (\text{K}) \tag{31.89}$$

where S_A is the heat dissipating area in cm^2 of the chosen core.

Example 31.6: ***Ferrite voltage transformer design***

Consider the design requirements for the split dc rail push-pull smps shown in figure 17.19b, which is specified as follows

v_o = 5 V
i_o = 4A
P_o = 20 W

V_s = 48 V ± 15 per cent
f = 20kHz
T_a = 25°C, $\Delta T \leq$ 35 K
η = 97 per cent (excluding secondary stage losses)

Solution

Based on the flowchart in figure 31.19 and the eleven stages outlined, design proceeds as follows.

Stage 1

The transformer must deliver 20 W plus losses associated with an output inductor and the pair of Schottky diodes in the output rectifier. The inductor loss is estimated at 4 per cent of the output power, 0.8 W, while the diode total loss is 0.6 V × 4 A = 2.4 W. Thus the transformer output power requirement P_s is 23.2 W (20 W + 0.8 W + 2.4 W). With a 97 per cent efficiency, the transformer input power, P_p, requirement is 1/97 per cent of 23.2 W, namely 23.9 W. The nominal primary current, I_p, at the nominal voltage, 24 V is

$$I_p = \frac{P_p}{V_{pn}} = \frac{23.9\text{W}}{24\text{V}} = 1\text{A}$$

The maximum primary voltage, V_p, is ½ ×1.15×V_{sec} = 27.6 V, since the 48 V supply is centre tapped and has + 15 per cent regulation. For worst case, it is assumed that the voltage drop across the switches is zero.

The transformer secondary voltage, V_{sec}, for the centre tapped full-wave rectifier circuit, must be large enough to overcome the diode voltage drop, V_d, and must allow for averaging of the nominal low duty

cycle switching action of the primary input power. With pwm regulation each input switch operates for approximately 25 per cent of the time, thus

$$½V_s = 2\times(V_o + V_d)$$

where the ½ indicates that half of the secondary winding conducts at any one time, while the 2 approximates the pwm average on-time. Thus for V_d = 0.6 V and V_o = 5 V

$$V_{sec} = 4\times(5+0.6) = 22.4\text{V}$$

Stage 2

Extracting the transformer data from stage 1

I_p = 1A	I_s = 4A
V_p = 27.6 V	V_{sec} = 22.4 V
P_p= 23.9 W	P_s = 23.2 W

η = 97 per cent, f = 20 kHz, T_a = 25°C, ΔT = 35 K

Stage 3

The total transformer power loss, P_L, from $P_s - P_p$, is 0.7 W.

Thus $P_c = P_{Cu} = ½\times 0.7$ = 0.35 W each.

Stage 4

The surface area requirement is calculated from equation (31.83)

$$S_A = 145\times\left[\frac{1000}{25+273}\right]^{2.06}\times\frac{0.7\text{W}}{35^{1.22}}$$

= 16.1 cm^2 for a 35 K temperature rise

Stage 5

Either the pot core in Table 31.5 or the pair of E-cores in figure 31.13 have sufficient surface area, 18.4 and 20 cm^2 respectively, and both are of a ferrite material suitable for a 10 to 100 kHz operating frequency range.

At the low power level of 23.9 W (<100W), choose the pot core.

Stage 6

Using the technical data given in Table 31.5, the core loss per unit volume is calculated

$$P_w = \frac{P}{V_e} = \frac{0.35\text{W}}{3.63\text{V}} = 0.096\text{W/cm}^3$$

Stage 7

From figure 31.8c, an operating flux density of 0.21 T at 20 kHz will result in the allowable core loss of 0.1 W/cm^3. For push-pull operation, the maximum allowable flux density is about 80 per cent of B_s, that is, 80 per cent of 0.48 T, namely 0.38 T.

Since 0.21 T < 0.38 T, a working flux density of 0.21 T is acceptable.

Stage 8

Since the operating flux density is greater than 100 mT, the pot core minimum area, A_{min} (0.95 cm^2) is used for calculations, rather than the effective area, A_e (0.999 cm^2). From equation (31.84), the required number of primary turns is given by

$$N_p = \frac{27.6\text{V}}{4\times 0.21\text{T}\times 0.95\times 10^{-4}\times 20\times 10^3} = 17.3$$

Use 17 turns.

The number of secondary turns is given by equation (31.85)

$$N_s = \frac{V_s}{V_p}N_p = \frac{22.4}{24}\times 17 = 15.7$$

where the nominal primary voltage is used. Use 16 turns per secondary winding.

Stage 9

From Table 31.5, the available winding area, A_N, is either 0.357 cm^2 for a one-section former or 0.266 cm^2 for a two-section former. Since the primary and secondary voltages are relatively low, insulation and isolation present few difficulties, hence single enamel copper wire and a single section former can be used. The available copper area, 0.357 cm^2, is divided between the primary and secondary so as to provide a uniform current density within the winding area. The primary to secondary currents are in the ratio of 1:4, hence 0.285 cm^2 is allocated to the secondary (approximately 80 per cent) while 0.072 cm^2 is allocated to the primary winding. The copper wire diameter is calculated using equation (31.86)

$$d_p = 2\sqrt{\frac{A_p k_w}{\pi N_p}} = 2\times\sqrt{\frac{0.072\times10^{-4}\times0.8}{17\pi}} = 0.66 \text{ mm}$$

$$d_s = 2\sqrt{\frac{A_s k_w}{\pi N_s}} = 2\times\sqrt{\frac{0.285\times10^{-4}\times0.8}{32\pi}} = 0.95 \text{ mm}$$

Using the standard wire tables in Appendix 31.12 and equation (31.75) to calculate the winding resistances

		Primary	Secondary	
d_{Cu}	mm	0.6	0.95	bare Cu
d_{Cu+en}	mm	0.65	1.017	single enamel
R_L	Ω/m	0.06098	0.02432	
R_{Cu}	Ω	0.055	0.0206/16 turns	

The total power copper loss is given by equation (31.88)

$$\begin{aligned} P_{Cu} &= I_p^2 R_p + I_s^2 R_s \\ &= 1^2\times0.055 + 4^2\times0.0206 \\ &= 0.055 + 0.330 = 0.385\text{W} \end{aligned}$$

Stage 10

The core loss is 0.35 W while the copper loss is only slightly higher at 0.385 W. No iterative change is necessary. The updated total loss, P_L, is 0.735 W.

Stage 11

The secondary power requirement remains 23.2 W while the primary requirement has increased to 23.94 W. The efficiency has been reduced to

$$\eta = \frac{23.3\text{W}}{23.94\text{W}} \equiv 96.9\,\text{per cent}$$

from 97 per cent.

Using the actual core surface area, 18.4 cm^2, and loss, 0.735 W, the core temperature rise can be calculated from equation (31.89)

$$\Delta T = 59\times\left(\frac{1000}{25+273}\right)^{1.69}\times\left(\frac{0.735}{18.4}\right)^{0.82}$$

$$= 32.6 \text{ K}$$

which is less than the 35 K allowable temperature rise limit.

♣

The transformer design of example 31.7 could be based on figure 31.18. The volume of the core plus copper, for the pot core in Table 31.5, can be estimated from its diameter of 25 mm and height of 16 mm. This yields a total volume of 6 cm^3, after allowing for slots.

Using figure 31.18, for a total volume of 6 cm^3, at 20 kHz, for a push-pull converter, 28 watts can be transmitted in a 20°C ambient, producing a 30 K core temperature rise. These results and those from example 31.6 compare as follows.

		Figure 31.18	Example 31.6
P	W	28	23.2
ΔT	K	30	32.6
T_a	°C	20	25

All other operating conditions are identical. Any design discrepancy is accounted for by

- the higher ambient temperature
- the poorer winding slot utilisation.

A centre tapped secondary represents poorer window slot utilisation compared with using a single winding, which requires four rectifying diodes since, because of a limited core size range, the same core would be used independent of the type of secondary circuit. A centred tapped secondary would result in the cost saving associated with two fewer Schottky diodes.

Transformer VA rating

The VA rating of a given transformer core need only be limited by Faraday's law, equation (31.84), and the current density in the coils. Faraday's equation uniquely specifies the number of turns, whence the VA rating is then only confined by the copper current density, *J*.

Faradays Equation

$$V_p = kfB_{\max}A_eN_p$$

where the primary and secondary electrical conditions are related by

$$\frac{V_s}{V_p} = \frac{N_s}{N_p} = \frac{I_p}{I_s}$$

The transformer core window accommodates both the primary and secondary windings, thus

$$k_wA_n = N_p\frac{I_p}{J} + N_s\frac{I_s}{J} = 2N_p\frac{I_p}{J}$$

The VA rating is

$$VA = V_pI_p\left(=V_sI_s\right)$$

Substituting for V_p and I_p

$$VA = kfB_{\max}A_eN_p \times \frac{Jk_wA_n}{2N_p}$$

$$P_{trans} = V \times A = ½k\Delta B_{op}A_ef \times JA_nk_w$$

where k_w is the copper winding or fill factor.

Transformer windings are usually designed to operate at less than 5% of the fusing current level of copper. The *VA* equation shows that a transformer can be exploited to transfer virtually limitless energy for short periods (a few seconds) by tolerating an extremely high copper current density, *J*. The penalty of briefly operating at a high percentage of the fusing current density of copper is the poor regulation due to the copper I^2R losses. The *VA* equation does not explicitly involve core length, which is a factor that determines magnetizing inductance. This design consideration is not a constraint when using nanocrystalline cores, at frequencies in excess of 1kHz, because of their extremely high relative permeability's, typically in excess of 30,000. Smaller cores can be used since 1T operation is possible.

31.6.2 Ferrite current transformer

By adding a secondary winding, a linear inductor can be converted into a voltage transformer, while a saturable inductor can be converted into a current transformer. The linear inductor and voltage transformer (of E-I laminations) are characterised by a core with an air gap (inherent in transformers which use E-I laminations). The saturable inductor and current transformer generally use an un-gapped core.

A given transformer can operate either in the voltage mode or the current mode depending on the load impedance. The voltage transformer operates into a high impedance circuit, while the current transformer requires a low impedance load. Current and voltage transformer action both cease at core saturation, and air coupling results in a low coupling factor, $k \rightarrow 0$.

The equivalent circuit model is identical for each transformer mode, and the same basic equations apply in each case. A saturable inductor is required to support a large voltage for a short period, while a current transformer supports a low voltage for a long period. In each case, the primary voltage-time product is equal for a given core and primary turns.

31.6.3 Current transformer design requirements

The basic requirement of a current transformer is a fixed ratio between the primary and secondary currents according to

$$I_pN_p = I_sN_s \quad \text{(A)} \tag{31.90}$$

Ideally the load impedance is zero, hence zero secondary voltage is developed. Practically, a secondary voltage, V_{sec}, exists (at least due to winding resistance), whence from Faraday's law

$$V_{\text{sec}} = N_s \frac{d\phi}{dt} = N_s A \frac{dB}{dt}$$

For a constant secondary voltage (a short circuit), the core flux density increases linearly, effectively moving up the *B-H* curve at a constant rate and reaches saturation, B_s, in time

$$t_s = \frac{N_s B_s A_e}{V_{\text{sec}}} \quad \text{(s)} \tag{31.91}$$

Where a core is operated with an *H* offset, for example, as with an inductor carrying dc current or a unidirectional current transformer, the maximum value of flux density used for analysis should be reduced because of remanence to B_s - B_r, whence

$$t_s = \frac{N_s \left(B_s - B_r\right) A_e}{V_{\text{sec}}} \quad \text{(s)} \tag{31.92}$$

The lower the secondary voltage, V_{sec}, the longer the time before saturation, (the lower the operating frequency in ac applications), at which point current transformer action ceases. The core is fully reset by a negative voltage of sufficient duration for which the voltage-time product must equal that *v-t* product of the on-period. Fortunately, a high reset voltage can generally be employed, which produces a short reset time. Effectively, the reset voltage forces the magnetising current, or more accurately, flux whence the stored energy, to zero.

This magnetising current, $\check{I}_p$ should be minimal and its presence modifies the ideal ampere-turns balance according to

$$\left(I_p - \check{I}_p\right) N_p = N_s I_s \quad \text{(A)} \tag{31.93}$$

where the magnetising current $\check{I}_p$ is given by

$$\check{I}_p = \frac{H \ell_e}{N_p} \quad \text{(A)} \tag{31.94}$$

The initial magnetising current is zero, and for a constant secondary voltage, increases linearly with time. Low leakage core shapes should be used to minimise leakage inductance.

At all times the primary voltage is related to the secondary voltage according to

$$V_p = V_{\text{sec}} \left(\frac{N_p}{N_s}\right) = \frac{V_{\text{sec}}}{n_T} \quad \text{(V)} \tag{31.95}$$

Table 31.6: Current transformer requirements showing how magnetic parameter variation affects electrical characteristics

		core parameters					*circuit parameters*		
		H_s	B_s	B_r	A_e	ℓ_e	N_s	N_p	V_{sec}
Equation (31.92) $t_s = \frac{N_s \left(B_s - B_r\right) A_e}{V_{\text{sec}}}$	s	*	↑	↓	↑	*	↑	↑	↓
Equation (31.94) $\check{I}_p = \frac{H_s \ell_e}{N_p} \frac{\hat{t}_{on}}{\check{t}_{off}}$	A	↓	*	*	*	↓	*	↑	*
Equation (31.98) $V_{sr} = V_p \frac{\hat{t}_{on}}{\check{t}_{off}}$	V	*	*	*	*	*	*	*	↓
$W = H_s \left(B_s - B_r\right) A_e \ell_e \left(\frac{\hat{t}_{on}}{t_s}\right)^2$	J	↓	↓	*	↓	↓	*	*	*
Design requirements		low H_s	—	low B_r	—	low ℓ_e	high turns		low V_{sec}

The requirements of the previous equations are summarised in Table 31.6 where the maximum on-time is $\hat{t}_{on}$, while the time available for reset is the minimum off-time $\check{t}_{off}$. The secondary reset voltage V_{sr} requirement and associated dissipated energy W are also included. This table summarises key current transformer requirements as follows

- use a core material which has a low magnetising force, H_s, at saturation
- use a core with a short effective core path length, ℓ_e
- use a high number of turns, N_p and N_s, for a given turns ratio
- operate the transformer with a low secondary voltage, V_{sec}.

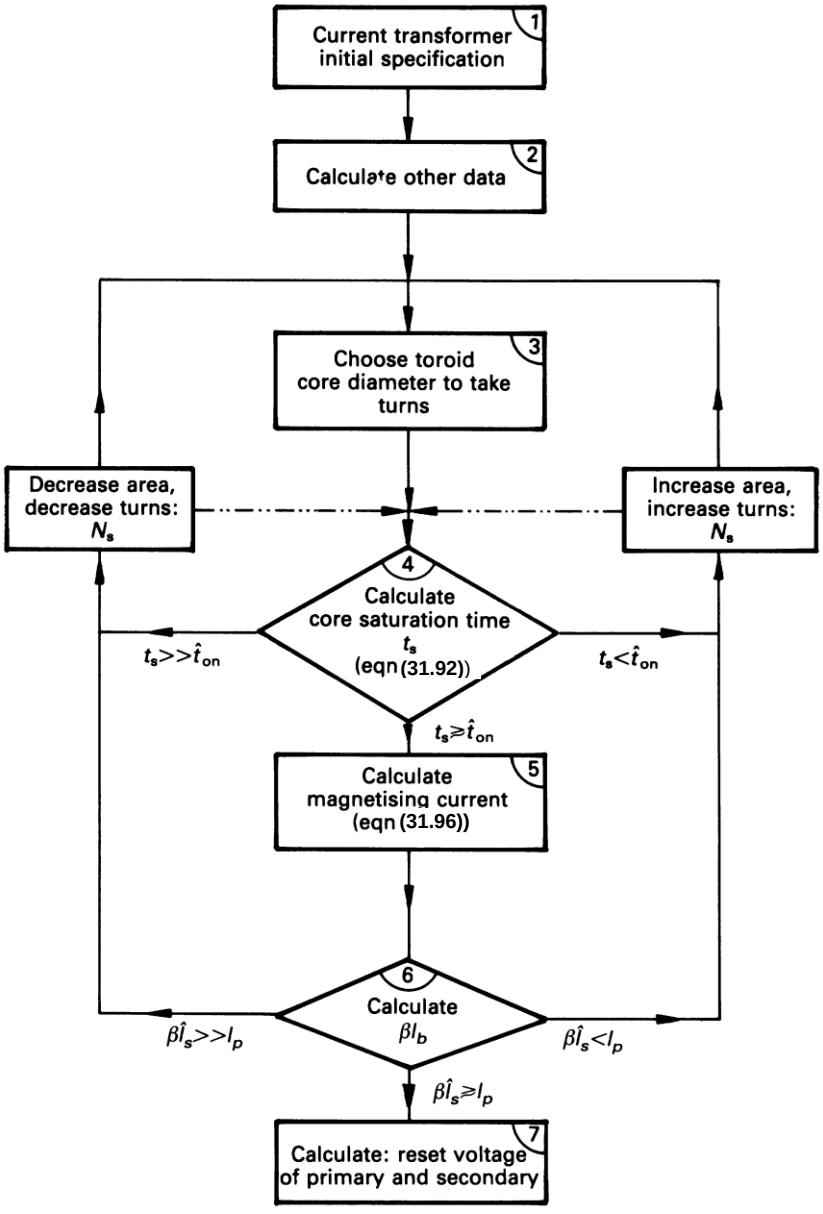

Figure 31.20. *Current transformer design flowchart.*

31.6.4 Current transformer design procedure

Figure 31.20 shows a flowchart design procedure for a current transformer and the design stages are as follows.

Stage 1/stage 2

The current transformer primary and secondary currents, hence turns ratio $n_T = N_s/N_p$, must be specified with the limits on duty cycle times, $\hat{t}_{on}$ and $\hat{t}_{off}$. The expected secondary voltage V_{sec} must be specified.

Stage 3

Select a ferrite toroid with an internal diameter, hence window area A_N, sufficient to accommodate the required minimum turns, $n_T + 1$. The copper turns current ratings must be taken into account. The core specifies the effective parameters ℓ_e, A_e, and V_e. The ferrite type specifies B_s, B_r, and H_s.

Stage 4

Calculate the time t_s, before the core saturates from equation (31.92). This time must be greater than the required maximum output current pulse width, $\hat{t}_{on}$.

(i) If $\hat{t}_{on} > t_s$
Either increase the number of turns, using a core with a larger window A_N if necessary.
or increase the core area, A_e, which can be achieved with the same window area, A_N, either with a core of increased thickness or by using two stacked cores.
go to stage 3

(ii) If $t_s >> \hat{t}_{on}$
Either decrease the number of turns which may allow a smaller core size.
or decrease the core cross-sectional area.
go to stage 3

(iii) If $t_s \gtrsim \hat{t}_{on}$, proceed to stage 5

Stage 5

Calculate the magnetising current at $\hat{t}_{on}$

$$\check{I}_p = \frac{H_s \ell_e \hat{t}_{on}}{N_p t_s} \quad \text{(A)} \tag{31.96}$$

Stage 6

Calculate the secondary current, taking the magnetising current $\check{I}_p$ into account

$$\hat{I}_s = \frac{\hat{I}_p - \check{I}_p}{n_T} \tag{31.97}$$

Is gain $\beta = \hat{I}_p / I_s$ sufficiently large?

(i) If $\hat{I}_p > \beta \hat{I}_s$
Either decrease the magnetising current by increasing core area.
or increase the turns ratio, n_T.
go to stage 3

(ii) If $\hat{I}_p \ll \beta \hat{I}_s$
Either decrease the turns ratio, n_T.
or decrease the core cross-sectional area.
go to stage 3

(iii) If $\hat{I}_p \lesssim \beta \hat{I}_s$, proceed to stage 7

Stage 7

Calculate the core reset voltage

$$V_{sr} = V_p \frac{\hat{t}_{on}}{\check{t}_{off}} \quad \text{(V)} \tag{31.98}$$

Calculate the reflected primary on-state voltage during core reset

$$e_p = \frac{V_{sr} N_p}{N_s} \tag{31.99}$$

Example 31.7: ***Ferrite current transformer design***

A current transformer primary is used in the collector of a SiC bipolar junction transistor switching circuit and the secondary is used to provide transistor base current as shown in figure 31.21. The maximum collector current is 100 A and the transistor has a gain of 8 at 100 A, in saturation ($v_{be\ sat}$ = 1.2V).

The transistor maximum on-time is 46 μs while the minimum off-time is 4μs. Design a suitable current transformer using the toroid ferrite core, which has low flux leakage and is specified by the data in Table 31.5 and Appendix 31.8. Assume a core temperature of 25°C.

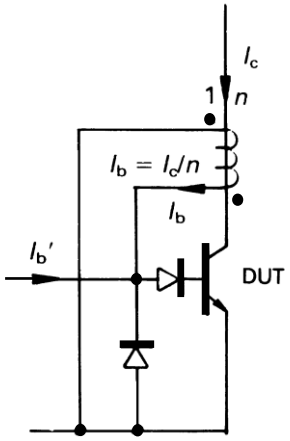

Figure 31.21. *Current transformer for BJT base drive.*

Solution

Based on the flowchart in figure 31.20 and the procedure previously outlined:

Stage 1

The required turns ratio factor is $n_T = N_p / N_s = \beta$ = 8/1. In allowing for the magnetising current component, choose n_T = 15/2.
The secondary winding voltage is the maximum transistor base to emitter voltage plus the maximum voltage drop across a series diode. Maximum voltage occurs at maximum current.

$$V_s = V_{be_{sat}} + V_D$$
$$= 1.2\text{V} + 1.2\text{V}$$
$$= 2.4\text{ V}$$

Stage 2

The current transformer requirements can be summarised as follows

$n_T = N_p / N_s = 15/2$ $\qquad \hat{t}_{on} = 46\mu\text{s}$

$V_{sec} = 2.4\text{V}$ $\qquad \hat{t}_{off} = 4\mu\text{s}$

Stage 3

The ferrite toroid core specified in Table 31.5, fulfils the following requirements

B_s = 0.4 T at H_s = 200 A/m

and $A = 0.398\text{ cm}^2$, $\ell_e = 9.71\text{cm}$

while the available window area, A_N, is 4.75 cm^2. This window must accommodate two conductor turns of 100 A (plus magnetising current) each and fifteen conductor turns of 12 A each.

Stage 4

The time, t_s, before core saturation is given by equation (31.92), and assuming flux density B_r = 0

$$t_s = \frac{15\times0.4\times0.4\text{T}\times10^{-4}}{2.4\text{V}} = 100\ \mu\text{s}$$

Since $t_s > \hat{t}_{on}$, that is 100μs > 46μs, proceed to stage 5.

Stage 5

The maximum primary magnetising current, $\hat{I}_p$ is specified by equation (31.96)

$$\hat{I}_p = \frac{46\mu s}{100\mu s} \times \frac{200 \times 9.71 \times 10^{-2}}{2} = 4.47A$$

Stage 6

The 4.47 A of magnetising current detracts from the primary current available for current transformer action. The maximum available secondary current under worst-case conditions is given by equation (31.97)

$$\hat{I}_s = \frac{100A - 4.47A}{15/2} = 12.7A$$

The maximum allowable collector current is this base current, 12.7 A, multiplied by the transistor gain, 8, which yields 102 A. This is larger than the specified maximum collector current of 100 A, hence the design is correct.

Stage 7

In the on-state, the secondary voltage is 2.4V and the reflected primary voltage is 0.32V.
The maximum secondary voltage, V_{sr}, required to reset the core is given by equation (31.98)

$$V_{sr} = 2.4V \times \frac{46\mu s}{4\mu s} = 27.6V$$

The reflected primary voltage is 3.7 V.
The available inherent circuit reset voltage is usually much larger, being clamped by a base circuit diode in avalanche. Therefore the core reset time will be shorter than 4μs.
At currents much lower than 100 A, the secondary voltage is decreased, hence the magnetising current is reduced. This reduced magnetising current could consume the full collector current at collector currents of a few amperes. It is therefore necessary to add extra base current to compensate for this deficiency at low currents. The minimum secondary voltage, V_{sec}, specifies the extra requirement according to

$$I_b' = \frac{\check{V}_s}{V_s} \times \frac{\hat{I}_p}{n_T} \qquad (31.100)$$

For $\check{V}_s$ = 1.2 V, the extra base current requirement is

$$I_b' = \frac{1.2}{2.4} \times \frac{4.47}{7.5} = 300mA$$

This current can be delivered from an inductive circuit since zero extra current is initially required, and the requirement rises linearly to 300mA in 46μs.
A base start pulse of a few microseconds duration is required initially to turn the transistor on, whence collector current is established and current transformer action commences, and is self-sustaining.

♣

31.7 Appendix: Soft ferrite general technical data

Tensile strength	20	N/mm^2
Flexural strength	40	N/mm^2
Resistance to compression	100	N/mm^2
Vickers hardness HV_{15}	800	N/mm^2
Modulus of elasticity	150,000	N/mm^2
Breakage modulus	80-120	N/mm^2
Thermal conductivity	4 - 7× 10^{-3}	J/mm s K (W/mm/K)
Linear expansion coefficient	7-10×10^{-6}	/K
Specific heat	0.75	J/g K
Density	4 - 5	g/cm^3 (4 per cent Si, 7.63 g/cm^3)
Porosity	5	%
Poisson ratio	0.28	pu

Resistivity ρ Ω cm	$\lambda_s = \frac{\Delta\ell^*}{\ell}$ ×10^{-16}	$\varepsilon_r^{\P} / \rho^{\S}(pu)$				
		10 kHz	100 kHz	1 MHz	100 MHz	300 MHz
10^5	-18	30/1	15/1	12/1	11/0.97	11/0.95
1	-1.5	140×10^3/1	50×10^3/0.95	30×10^3/0.65	-	-

* Magnetostriction, at saturation, contraction.
¶ Dielectric constant, $\varepsilon_r \rightarrow$ 10-20 at high frequency.
§ Resistivity normalised at low frequency.

31.8 Appendix: Technical data for a ferrite applicable to power applications

Symbol	Unit	Test condition	#1	#2
μ_i		25°C	2500±20%	2200±25%
$\hat{B}$	T T	25°C 100°C	0.48 0.37	0.54 0.45
H_s	A/m	B_s, 25°C	B_s = 0.4T : 200	B_s = 0.5T : 200
H	A/m		1600	
H_c/B_r	A/m /T	25°C 100°C	12/0.18 9.6/0.11	13/0.17 6.5/0.06
α/β	%/°C	Rev temp coeff	-0.11/-0.2	-0.11/-0.2
T_c	°C		> 200	> 250
ρ	Ω cm		100	700
η_B^*	mT^{-1} × 10^{-6}	10 kHz	0.9	
Density	g/cm^3		4.8	4.9
f_c	MHz	25°C	1.8	1.6

* - Maximum hysteresis coefficient
10 G (gauss) = 1 mT (milliTesla)
10 *e* = 80A/m

31.9 Appendix: Technical data for Iron, nickel, and cobalt applicable to power applications

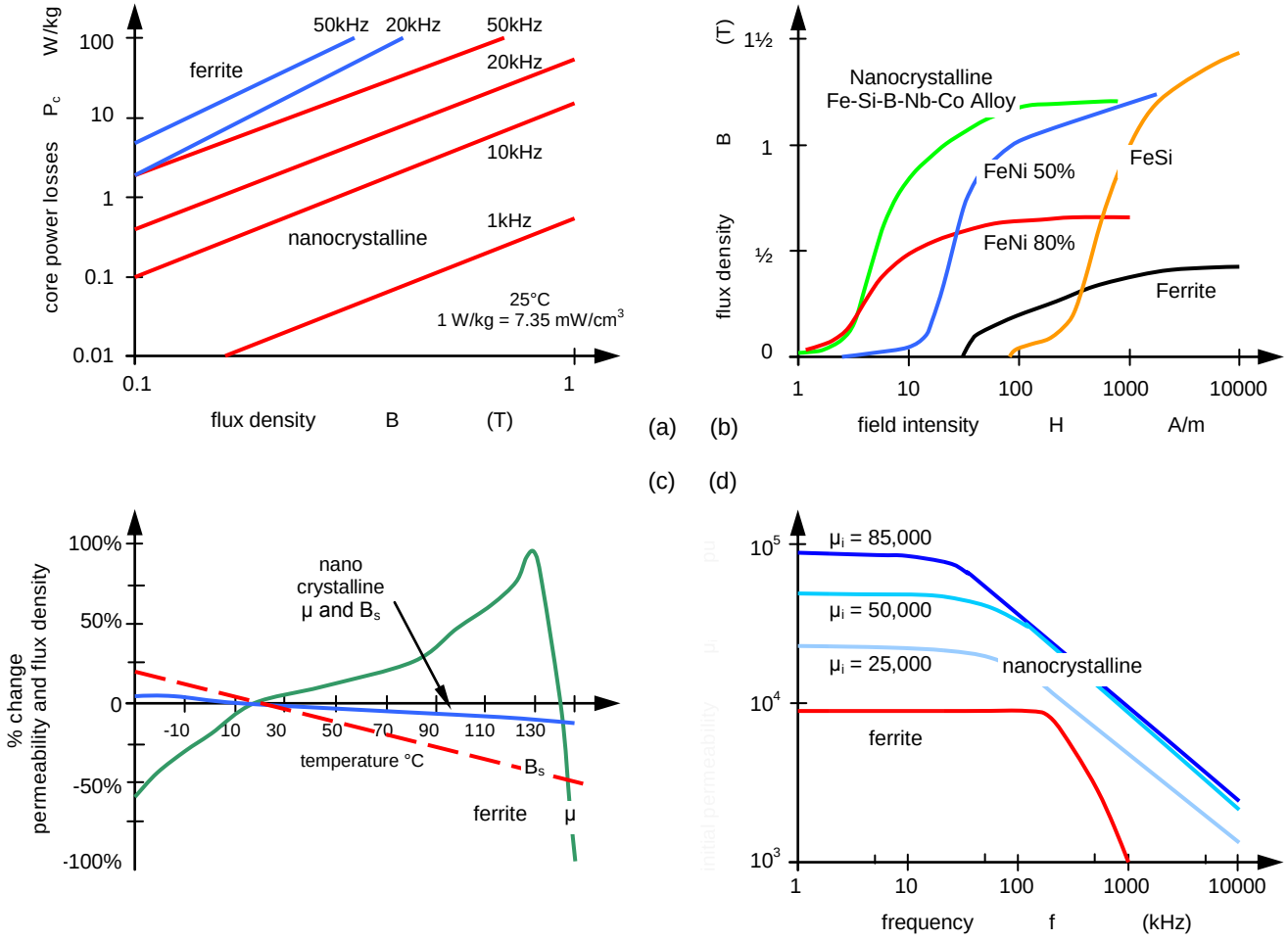

Figure 31.22. *Typical Fe-Si nanocrystalline material characteristics: (a) core losses; (b) B-H curves; (c) temperature dependence; and (d) permeability dependence on frequency.*

alloy	grain size	saturation flux density	saturation magnetostriction	coercivity	initial permeability	electrical resistivity	core losses	ribbon thickness
	d	B_s	λ_s	H_c	μ_i	ρ	P_c	t
	nm	T	10^{-6}	A/m		μΩcm	W/kg	μm
					@ 1 kHz		0.2T 100kHz	
$Fe_{73.5}Si_{15.5}$	14	1.23	0	0.4	100,000	115	35	21
$Fe_{84}Nb_7B_9$	9	1.49	0.1	8	22,000	58	76	22
$Fe_{86}Cu_1Zr_7B_6$	10	1.52	0	3.2	48,000	56	116	20
$Fe_{91}Zr_7B_3$	17	1.63	-1.1	5.6	22,000	44	80	18
$Co_{68}Fe_4(MoSiB)_{28}$	amorphous	0.55	0	0.3	150,000	135	35	23
$Fe_{76}(SiB)_{24}$	amorphous	1.45	32	3	8,000	135	50	23
80% Ni-Fe	100,000	0.75	1	0.5	100,000	55	90	50
50% Ni-Fe	100,000	1.55	25	5	40,000	45	200	70

31.10 Appendix: Eddy currents, skin effect, and proximity effect

Two independent effects are associated with a conductor is carrying an alternating current:

- ***skin effect***: ac current in a conductor generates *internal B - field* which influences its current
- ***proximity effect***: ac current in one conductor generates *external B – field* which makes current flow in a second conductor.

From electromagnetic wave theory, a conductor that carries current will generate both internal and external electromagnetic fields.

That is, from $\oint_s H.d\ell = \iint_A J.dA,$ for a conductor of radius, *r*, carrying current *I*:

$$B_{in}(x) = \frac{\mu_o I}{2\pi r^2} \times x \qquad x \le r \qquad \text{inside conductor}$$
$$B_{out}(x) = \frac{\mu_o I}{2\pi} \times \frac{1}{x} \qquad x \ge r \qquad \text{outside conductor} \tag{31.101}$$

The primary field energy produced will be focused outside the conductor because all time-varying fields attenuate rapidly within a good conductor. A conductor carrying dc current or low frequency ac current will generate a field external to the conductor that is radially symmetrical, concentric. This symmetrical field forces current within the conductor to distribute itself uniformly throughout the conductor. With uniform current flow, the effects of skin and eddy are negligible. Thus skin effect and the effects of eddy currents are considered high frequency phenomenon.

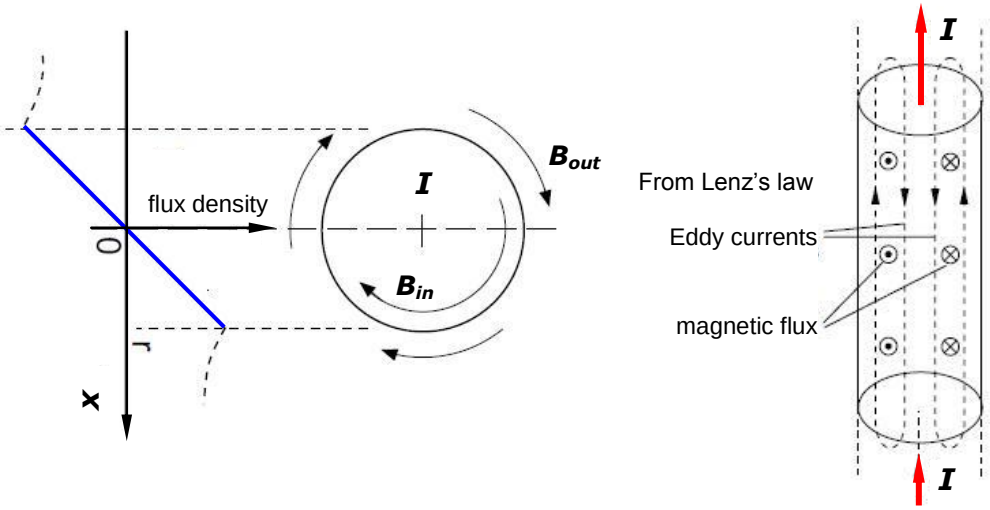

Figure 31.23. *Current induce fields:*
(a) conductor internal and external magnetic fields, B and (b) Eddy currents in a round conductor.

Eddy currents

At frequencies above 20kHz, the current inside the conductor changes direction rapidly. This rapid current change causes rapid flux changes within the conductor. Flux change ($d\phi/dt$) induces a voltage loop, termed an eddy loop, close to the surface of the conductor. The induced voltage forces a current to flow coincident with the voltage. This current is known as eddy current. This current loop will be additive to current flowing near the surface and oppose current in the centre of the conductor. The result is that the current density increases at the surface and decreases toward the centre of the conductor. There is an exponential decrease in the conductor current density and electric field intensity with penetration into the conductor.

Skin depth is defined as the distance from the surface to where the current density is 1/e times the surface current density. One skin depth is where the current density has decreased by approximately 37% (1/e) of the surface current density. The following frequency dependant expression (equations (31.50) and (31.123)) is used to calculate the skin depth of a conductor:

$$\delta_{pen} = \sqrt{\frac{\rho}{\pi \mu_o \mu_c f}}$$

where ρ is conductivity, 2.3 X 10-6 Ω-cm for 100°C copper, and $\mu_o = 4\pi \times 10^{-7}$.

Since skin depth is related to conductivity, skin depth is temperature dependant, increasing with increased temperature. Although Litz wire (thin weaved wires of diameter of less than 2δ) can minimise the skin effect (decrease ac resistance), the external proximity effect favours twisted bundling.

Proximity Effect

Particularly in low voltage equipment, proximity, or the closeness of other current carrying conductors to the principal conductor, affects the ability of that conductor to carry current. The fields of the conductors in close proximity will add and subtract depending on their direction. In circuit components such as circuit boards and magnetic devices, special attention has to be given to these effects, minimizing their high frequency adverse effects. When two conductors are in close proximity, their external electro-magnetic fields may add or subtract. High frequency current will concentrate within the wire where the fields are additive. Thus, like skin effect, a further distortion of current density results from the interaction of the magnetic fields of other close proximity conductors, limiting the effective capability of a wire to conduct high frequency currents.

In the same way as an emf may be induced in a conductor by its own magnetic flux, so may the magnetic flux of one conductor produce an emf in any other conductor sufficiently near for the effect to be significant. If two such conductors carry currents in opposite directions, their electro-magnetic fields oppose one another and tend to force one another apart. This results in a decrease of flux linkages around the adjacent parts of the conductors and an increase in the more remote parts, which leads to a concentration of current in the adjacent parts where the opposing emf is a minimum. If the currents in the conductors are in the same direction the action is reversed and they tend to crowd into the more remote parts of the conductors.

Condition for Minimum Loss

The 'proximity effect', or 'shape effect', tends usually to increase the apparent ac resistance.

Both skin and proximity effects are due to circulating or 'eddy' currents caused by the differences of inductance which exist between different 'elements' of current-carrying conductors. The necessary condition for avoidance of both these effects (and hence for minimum loss) is that the shapes of each of the conductors in a single-phase system approximates to 'equi-inductance lines'. For close spacing, rectangular section conductors most closely approach the ideal. Such an arrangement is also convenient where space is limited and where inductive voltage drop due to busbar reactance must be reduced to a minimum. In the case of heavy current single-phase busbars and where space is slightly less restricted, the single channel arrangement gives the closest approximation to the equi-inductance condition, the channels of 'go' and 'return' conductors being arranged back-to-back, while for wider spacing a circular section is preferable.

In some cases, however, the proximity effect may tend to neutralise the skin effect and produce a better distribution of current as in the case of strip conductors arranged with their flat sides towards one another. If the conductors are arranged edgewise to each other the proximity effect increases. In most cases the proximity effect also tends to increase the stresses set up under short-circuit conditions and this may therefore have to be taken into account.

The unbalancing of current due to the proximity effect can be reduced by spacing the conductors of different phases as far apart as possible and sometimes by modifying their shape in accordance with the spacing adopted. In the case of laminated bars, a reduction may be obtained by transposing the laminations at frequent intervals or by employing current balancers using inductances.

Proximity effect may be completely overcome by adopting a concentric arrangement of conductors with one inside the other as is used for isolated phase busbar systems.

The magnetic field round busbar conductors may be considerably modified and the current distortion increased by the presence of magnetic materials and only metals such as copper or copper alloys should be used for parts likely to come within the magnetic field of the bars.

31.11 Appendix: Cylindrical inductor design

Figures 31.24a and b show cross-sectional views of single-layer and multi-layer cylindrical inductors. The inductance of a single-layer cylindrical inductor (all dimensions are in mm) is given by

$$L = \frac{\mu_{eff}\ r^2 N^2}{228.6r + 254\ell} \qquad (\mu H) \qquad (31.102)$$

while if the insulation spacing between the single layer turns are accounted for, inductance is given by

$$L = \frac{\frac{2}{3}\mu_{eff} N^{1.3} \left(d + d_w\right)^{1.7}}{\left(d_w + S\right)^{0.7}} \qquad (nH) \qquad (31.103)$$

where the bare wire diameter is d_w and S is the spacing between turns, both in mm.

For the multi-layer cylindrical inductor shown in figure 31.24b, inductance is given by

$$L = \frac{\mu_{eff}\ r^2 N^2}{152.4r + 228.6\ell + 254b} \qquad (\mu H) \qquad (31.104)$$

Figure 31.24d shows a family of curves used to give the effective permeability from the former *l*/*d* ratio and the core material permeability. These curves are applicable to the single-layer inductor but are a fair approximation of the multi-layer inductor. The winding is assumed to be closely wound over 95 per cent of the core length.

The inductance of a flat spiral air-core coil as shown in figure 31.24c is virtually independent of any axial core and is given by

$$L = \frac{r^2 N^2}{203r + 279b} \qquad (\text{mH}) \qquad (31.105)$$

For inductance levels below 100 μH, an air core strip wound inductor as shown in figure 31.24e, has an inductance approximated by

$$L = \frac{r^2 N^2}{225r + 250\ell + 250b + 82.5\dfrac{\ell b}{r}\left(\dfrac{\ell + 2r}{\ell + 4r}\right)} \qquad (\mu H) \qquad (31.106)$$

A toroidal core with a circular cross section has inductance given by

$$L = \mu_o \mu_{eff} \frac{r^2 N^2}{D} \qquad (\text{H}) \qquad (31.107)$$

where *r* is the radius of the coil winding and *D* is the overall diameter of the toroid, all in metres.
Inductor design using these equations may require an iterative solution. Always attempt to maximise the winding surface area ($S_A \approx \pi(d + 2b)\ell$) for better cooling.

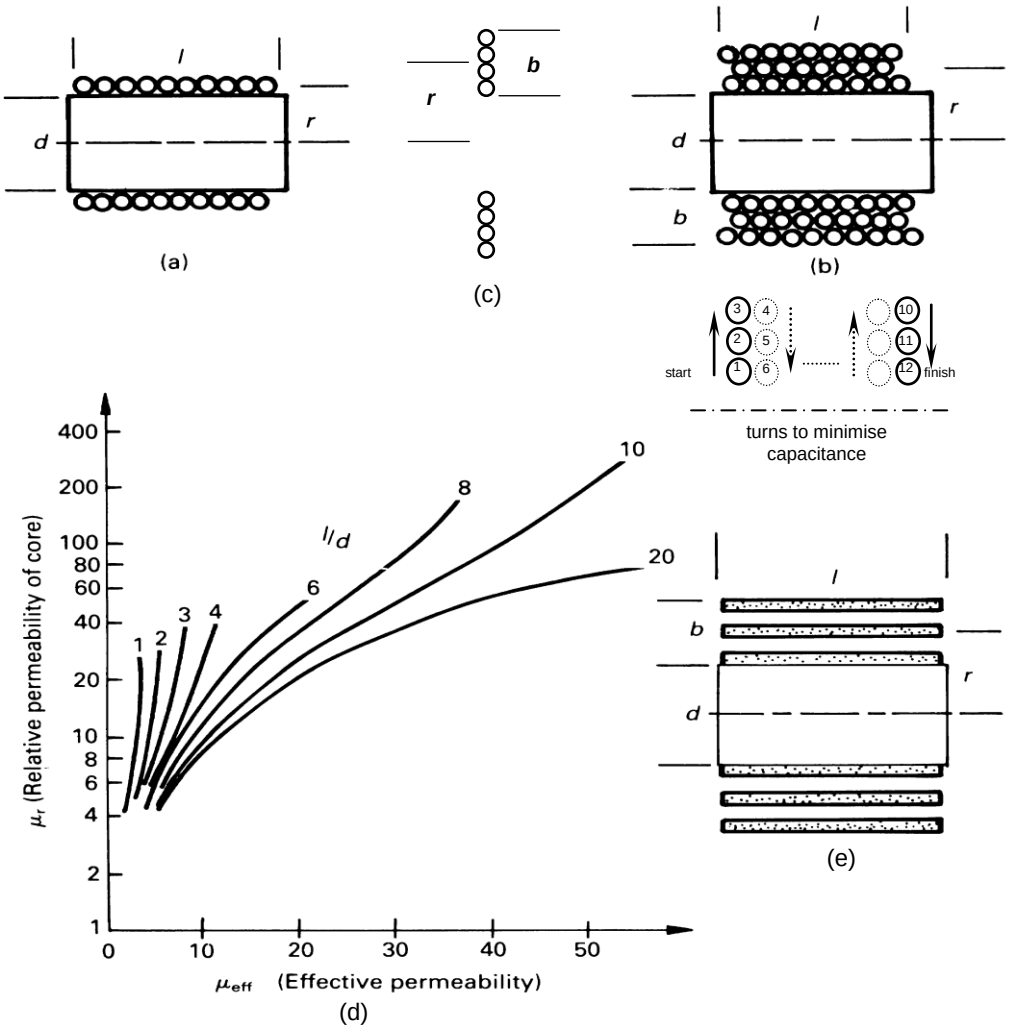

Figure 31.24. *Cylindrical inductors: (a) single-layer coil; (b) multi-layer coil; (c) coil layer; (d) effective permeability for different aspect ratios, l/d; and (e) core strip wound air core inductor.*

Example 31.8: *Wound strip air core inductor*

An air core inductance of 50 μH is made as a wound strip of copper, 40 mm wide and 1.5 mm thick. For cooling purposes, ½ mm spacing is used between each turn with an inner diameter of 60 mm and an outer diameter of 160 mm as physical constraints: Can the required inductance be achieved?

Solution

First calculate the parameters shown in figure 31.24e.

$$r = \tfrac{1}{4}\left(d_o + d_i\right) = \tfrac{1}{4} \times \left(160 + 60\right) = 55 \text{ mm}$$

$$b = \tfrac{1}{4}\left(d_o - d_i\right) = \tfrac{1}{4} \times \left(160 - 60\right) = 25 \text{ mm}$$

$$\ell = 40 \text{ mm}$$

$$N = \frac{b}{t_{Cu} + t_{air}} = \frac{50}{1.5 + 0.5} = 25 \text{ turns}$$

Substitution of the appropriate parameters values into equation (31.106) yields L = 51.6 μH.

♣

Example 31.9: *Multi-layer air core inductor*

An air core inductor is to have the same dimensions as the inductor in example 31.8. The same conductor area (40 mm × 1.5 mm) but circular in cross-section and number of turns is to be used. Calculate the inductance. If a ferrite solid cylindrical core 42 mm long and 60 mm in diameter with a relative permeability of 25 is inserted, what will the inductance increase to?

Solution

From example 31.8

r = 55 mm $\quad\quad$ ℓ = 40 mm

b = 50mm $\quad\quad$ N = 25

Substitution of these parameter values into equation (31.104) yields 62.5 μH.

From figure 31.24c, ℓ / d = 40/60 = 0.66, whence $\mu_{eff} \approx 3$. That is, with a cylindrical core inserted, a three fold increase in inductance would be expected (188 μH).

The use of end-caps and an outer magnetic sleeve would increase inductance, but importantly also help to contain the external magnetic field.

♣

31.12 Appendix: Copper wire design data

Nominal wire diameter d	Outer diameter enamelled grade 2	Approximate dc resistance at 20°C	Bare copper weight	Fusing current
mm	mm	Ω/m	gm/m	A
0.1	0.129	2.195	0.070	2.5
0.2	0.245	0.5488	0.279	7
0.376	0.462	0.136	1.117	18
0.5	0.569	8.781×10^{-2}	1.746	27.5
0.6	0.674	6.098×10^{-2}	2.50	36
0.8	0.885	3.430×10^{-2}	4.469	57
0.95	1.041	2.432×10^{-2}	6.301	79
1	1.093	2.195×10^{-2}	6.982	82
1.5	1.608	9.67×10^{-3}	15.71	145
2	2.120	5.44×10^{-3}	27.93	225
2.5	2.631	3.48×10^{-3}	43.64	310
3	3.142	2.42×10^{-3}	62.84	>
4	4.160	1.36×10^{-3}	111.7	>
4.5	4.668	1.08×10^{-3}	141.4	>
5.0	5.177	8.70×10^{-4}	174.6	>

31.13 Appendix: Minimisation of stray inductance

In many circuit layouts, it is essential to minimise stray and residual inductance. With high *di/dt* currents during switching, large voltages occur ($v = L\ di/dt$) which may impress excessive stresses on devices and components. Stray inductance within a package reduces its usable voltage rating. Stray inductance in the drain circuit of the MOSFET, within the package as shown in figure 4.11, reduces the usable voltage rail while source inductance increases the transient gate voltage. In the case of capacitors, residual inductance reduces the effectiveness of turn-off snubbers and can result in an unintentional resonant circuit.

Inductance of a straight wire of length ℓ and radius r is

$$L = \frac{\mu_o \ell}{2\pi}\left(\ell n \frac{2\ell}{r} - ¾\right) \quad \text{(H)} \quad \text{or} \quad L = 0.2\ell\left(\ell n \frac{2\ell}{r} - ¾\right) \quad (\mu\text{H}) \tag{31.108}$$

which as a rule of thumb is about 1μH/m.

31.13.1 Reduction in wiring residual inductance

Wiring inductance can be decreased by cancelling magnetic fields in a number of ways

- coaxial cable
- parallel plates
- parallel wiring conductors.

In each case, the go and return paths are made parallel and physically close. Figure 31.25 shows the per unit length inductance for each wiring method.

coaxial cable

Minimum inductance results with coaxial cable, which is available for power application. The per unit inductance and capacitance are given by

$$\begin{aligned} L &= \frac{\mu_o \mu_r}{2\pi} \ell n \frac{r_o}{r_i} \quad \text{(H/m)} \\ C &= 2\pi\varepsilon_o\varepsilon_r \,/\, \ell n \frac{r_o}{r_i} \quad \text{(F/m)} \end{aligned} \tag{31.109}$$

where r_i is the inner radius and r_o the outer radius ($r_i < r_o$).

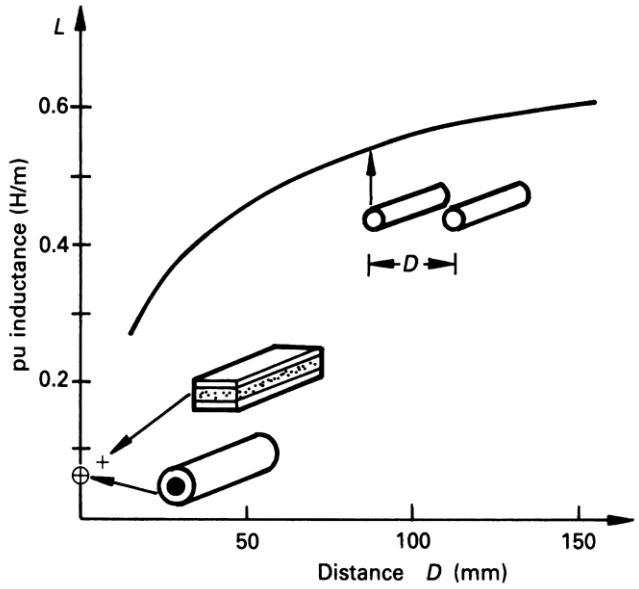

Figure 31.25. *Relative inductance of go and return wiring conductors.*

parallel plates

Low inductance can be achieved by using parallel conducting copper plates separated by a thin insulation layer ($\mu_r \approx 1$). The inductance per unit length, neglecting skin effects, is approximated by

$$L = \mu_o \frac{d}{w} \quad \text{(H/m)} \quad (w >> d) \tag{31.110}$$

where d is the separation of the plates and
w is the plate width.

The parallel plate capacitance is

$$C = \varepsilon_o \varepsilon_r \, w / d \qquad \text{(F/m)} \tag{31.111}$$

A complete analysis of the laminated parallel bus bar configuration is presented in Appendix 31.14

parallel wiring conductors

For parallel wiring cylindrical conductors of radius r and separation D, in air,

$$L_{lo-freq} = \frac{\mu_o}{\pi} \ell n\left(\frac{D}{r}\right) \qquad L_{hi-freq} = \frac{\mu_o}{2\pi} \cosh^{-1}\left(\frac{D^2}{2r^2} - 1\right) \qquad (\text{H/m}) \qquad (D > 2r)$$

$$C = \frac{2\pi\varepsilon_o}{\ell n\left(\frac{D}{r}\right)} \qquad \text{(F/m)} \tag{31.112}$$

When the separation D is small over a long distance, ℓ, that is $D/\ell << 1$, the inductance, mutual coupling inductance, and capacitance, are

$$L = \frac{\mu_o}{\pi}\left\{\ell n\left(\frac{D}{r}\right) - \frac{D}{\ell} + ¼\right\} \qquad (\text{H/m})$$

$$M = \frac{\mu_o}{2\pi}\left\{\ell n\left(\frac{D}{r}\right) - \frac{D}{\ell} - 1\right\} \qquad (\text{H/m}) \tag{31.113}$$

$$C = \frac{\pi\,\varepsilon_o}{\cosh^{-1}\left(\frac{D}{2r}\right)} \qquad \text{(F/m)}$$

At high frequencies, the inductance per unit length of a pair of parallel wires is better estimated by

$$L = \frac{\mu_o}{2\pi} \cosh^{-1}\left(\frac{D^2}{2r^2}\right) \qquad (\text{H/m}) \tag{31.114}$$

parallel wiring conductors over a conducting ground plane

The self inductance and mutual inductance between two conductors height h over a ground plane carrying the return current are given by

$$L_{lo-freq} = \frac{\mu_o}{2\pi} \ell n \frac{2h}{r} \qquad L_{hi-freq} = \frac{\mu_o}{4\pi} \cosh^{-1}\left(\frac{2h^2}{r^2} - 1\right) \qquad \text{(H/m)}$$

$$M = \frac{\mu_o}{4\pi} \ell n\left(1 + \left(\frac{h}{r}\right)^2\right) \qquad \text{(H/m)} \tag{31.115}$$

$$C = ½ \frac{2\pi\varepsilon_o}{\ell n\left(\frac{D}{r}\frac{2}{\sqrt{D^2 + 4^2}}\right)} \qquad \text{(F/m)}$$

At high frequencies, the inductance per unit length of a wire parallel to a conducting wall is better estimated by

$$L = \frac{\mu_o}{2\pi} \cosh^{-1}\left(\frac{D^2}{2r^2}\right) \qquad (\text{H/m}) \tag{31.116}$$

Figure 31.25 shows that go and return power cable residual inductance decreases as separation decreases. Physical and mechanical constraints may dictate which wiring technique is most viable. All other wiring should cross perpendicularly, in order to minimise coupling effects.

Inductance of other conductor profiles

The self-inductance of a rectangular conductor, not associated with a return path in close proximity is

$$L = \frac{\mu_o}{2\pi}\left[\ell n\left(\frac{2\ell}{w + t}\right) + ½ + \frac{2}{9}\frac{w + t}{\ell}\right] \qquad \text{(H/m)} \tag{31.117}$$

When the bus bar and its return path are side-by-side in the same plane

$$L = \frac{\mu_o}{2\pi}\left[\ell n\left(\frac{D}{w+t}\right)+\frac{3}{2}\right] \quad \text{(H/m)}$$
$$M = \frac{\mu_o}{2\pi}\left[\ell n\left(\frac{2\ell}{D}\right)-1+\frac{D}{\ell}\right] \quad \text{(H)} \qquad (31.118)$$

or long cylindrical wire and its return path are side-by-side in the same plane

$$L = \frac{\mu_{wire}}{8\pi}+\frac{\mu}{2\pi}\ell n\frac{D}{r} \quad \text{(H/m)} \qquad (31.119)$$

where w is the width of the conductors
t is the thickness of the conductors
D is the distance between the midpoints of the conductors
ℓ is the conductor length.

The first component in equation (31.119) is the internal self-inductance component, which for copper and aluminium, $\mu_{wire} = \mu_o$, gives 50nH per metre.

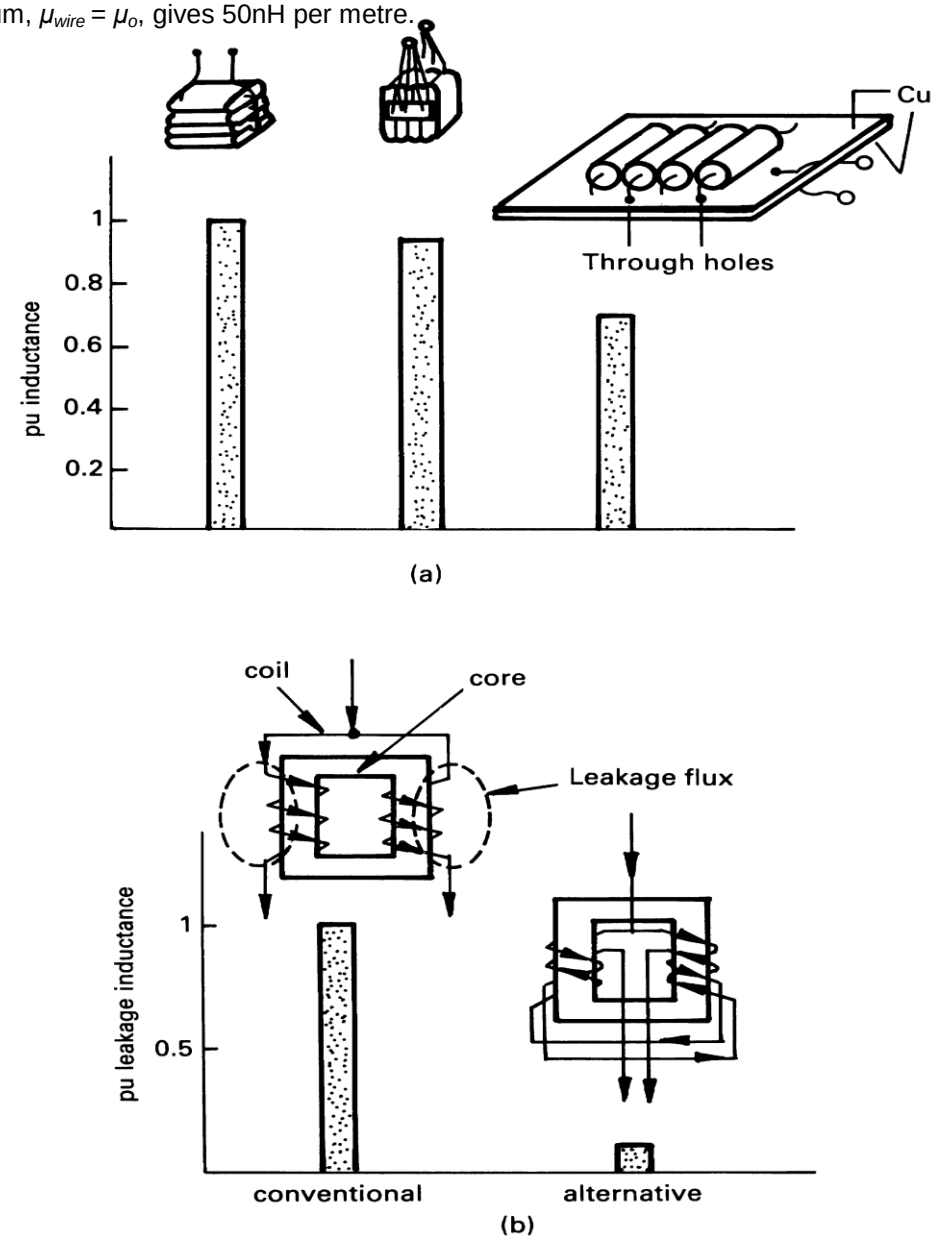

Figure 31.26. *(a) Parallel connected capacitors, inductance and (b) leakage inductance of a current balancing transformer.*

31.13.2 Reduction in component residual inductance

31.13.2i - Capacitors

The inductance of a cylindrical capacitor winding, employing extended foils and scooping connections is given by

$$L = \frac{\mu_o}{2\pi}\left[\ell n \frac{2b}{r} - \tfrac{3}{4}\right] \quad \text{(H)} \qquad (31.120)$$

where *b* is the length of the cylinder winding and *2r* is its diameter. This equation shows that (undesirable) inductance is decreased by decreasing the length and by increasing the diameter.

31.13.2ii - *Capacitors - parallel connected*

Capacitors are extensively parallel connected, by manufacturers before potting, or by the user after potting, in order to increase capacitance. The low inductance feature of an extended foil, scoop connected capacitor can be obliterated by poor lead connection. Consider the parallel-connected capacitors shown in figure 31.26a, which shows the relative residual wiring inductance for three connections. Minimum inductance results when using a thin, double-sided copper printed circuit board arrangement, such that connections alternated between the top and bottom copper layers (go and return conductors). Cut-outs in the pcb, for the capacitors to fit into, only marginally decrease the inductance.

31.13.2iii - *Transformers*

A current balancing transformer may be used to equalise the principal currents of two parallel-connected power devices, as shown in figure 11.8. Conventionally each coil is wound on separate legs of the core, resulting in a large leakage inductance. This large leakage inductance can result in high voltage transients, which are to be avoided.
Leakage can be significantly decreased if two coils are bifilar wound on each limb and connected as shown in figure 31.26b. The same leakage flux cancelling technique can be used on the centre-tapped, push-pull transformer for the switch mode power supply shown in figure 19.16a. Because of the close proximity of bifilar wound conductors, high inter-winding capacitance and high dielectric fields may be experienced.

31.14 Appendix: Laminated bus bar design

As shown in figure 31.25, the use of a parallel laminated bus bar arrangement shown in figure 31.27a for go and return paths, results in a low inductance loop. If the gap between the bus bars is laminated with a dielectric material (e.g., polyester, ε_r = 3.5, $10^{18}\Omega$ insulation resistance, and a dielectric strength of 300kV/mm), distributed capacitance properties are gained. Up to five layers are available.

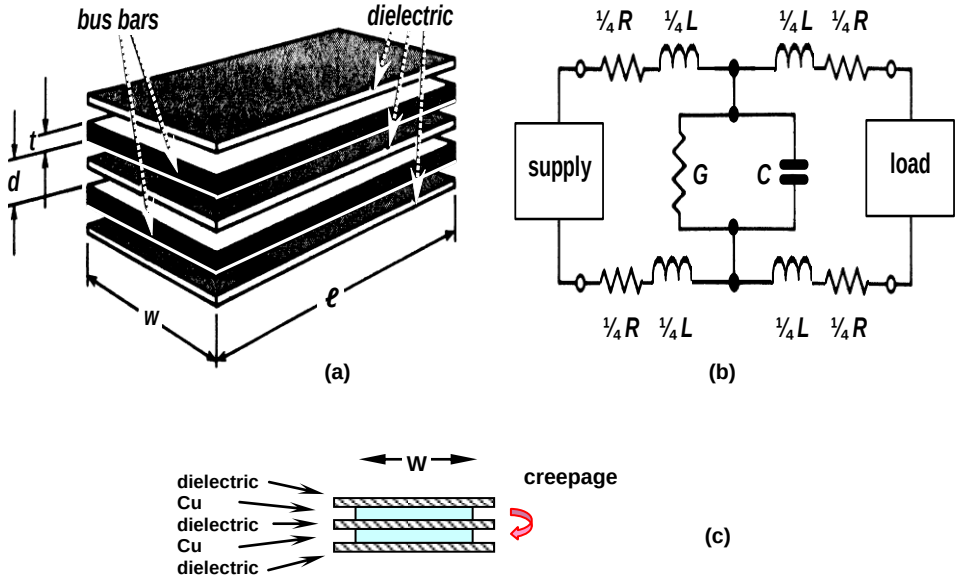

Figure 31.27. *Laminated bus bar:*
(a) parallel planar construction; (b) equivalent circuit distributed components; and (c) cross section showing creepage paths between copper conductors.

A laminated bus bar arrangement offers the following electrical mechanical and economic features in mitigation to the increased component costs:

- high packing density with good shielding
- better conductor cooling and thermal distribution because of flat surface area
- low voltage drop - low impedance

- high voltage and current capability
- modular, reliable, and eliminates wiring errors
- space saving, high packing density, low profile, low weight, and high mechanical strength
- increased capacitance for better noise suppression
- low inductance because thin parallel conductors allow flux cancellation
- low system costs, easy but low service costs, low installation costs
- applicable to voltages up to and in excess of 1kV

The physical bus bar dimensions determine the electrical parameters and characteristics. The two level bus bar comprises two parallel conducting plates of aluminium, brass or copper with resistivity σ, separated by a dielectric, with dielectric constant ε_r, and permeability μ_o, giving a conductance *G*, capacitance *C*, and resistance *R* that are uniformly distributed along the bus, as shown in the model in figure 31.27b.

Capacitance, C

The capacitance *C* is given by

$$C = \varepsilon_o \varepsilon_r \frac{w}{d} \qquad \text{(F/m)} \qquad (31.121)$$

where *w* is the width of the conductors
d is the distance between the bars, which is the dielectric thickness.

An increase in capacitance decreases the characteristic impedance, $Z_o = \sqrt{L/C}$. Lower impedance gives greater effective signal suppression and noise elimination. This is achieved with

- a smaller bar separation, *d*,
- a higher permittivity dielectric material, ε_r,
- wider conductors, *w*.

Shunt conductance, G

The shunt conductance *G* depends on the quality of the dielectric, specifically its conductivity at the operating frequency and temperature.

$$G = \frac{1}{\sigma}\frac{w}{d} \qquad \text{(℧/m)} \qquad (31.122)$$

Skin effect

Both the resistance and inductance are affected by the ac skin effect, which is frequency dependant. This was briefly treated in section 31.3.4ii, and specifically equation (31.50). The skin effect is when at high frequencies the current tends to flow on the surface of the conductor. The skin depth δ, from equation (31.50) is

$$\delta(f) = \sqrt{\rho / \mu_o \pi f} \qquad (31.123)$$

where ρ is the resistivity of the conductor at frequency *f* and a given temperature.

The skin depth for copper and brass are

$$\delta_{Cu} = \frac{0.066}{\sqrt{f}} \quad \text{(m)} \qquad \delta_{Brass} = \frac{0.126}{\sqrt{f}} \quad \text{(m)} \qquad (31.124)$$

As the frequency increases *L* decreases and *R* increases.

Inductance, L

There two inductive components,

- L_{int} - inside the conductor due to internal flux linkages,
- L_{ext} - external inductance between the two conductors due to the orientation of the two conductors carrying current.

In power applications and at the associated frequencies, the external inductance is more dominant.

$$L_{ext} = \mu_o \frac{d}{w} \qquad \text{(H/m)} \qquad (31.125)$$

At high frequency (taking the skin effect into account) the effective inductance is

$$L_e = \mu_o \frac{d+\delta}{w} \qquad \text{(H/m)} \qquad (31.126)$$

Thus to decreased inductance

- decrease the dielectric thickness, *d*
- increase the conductor width, *w*
- decrease the skin depth δ by using a conductor of lower resistivity.

Resistance, R

The dc resistance R_{dc} of the two conductors is

$$R_{dc}(20°\text{C}) = 2\rho\frac{1}{w\,t} \quad (\Omega/\text{m}) \tag{31.127}$$

where *t* is the thickness of the conductors

The resistivity of copper and brass at 20°C are 1.7×10^{-8} and 7.0×10^{-8} Ωm, respectively.

The temperature effects on resistance for copper are accounted for by

$$R_{T_o} = R_{20°C}\left(1 + 0.0043\times\left(T_o - 20°C\right)\right) \quad (\Omega) \tag{31.128}$$

At high frequency, taking the skin effect into account, assuming that the conductor thickness is at least twice the skin depth,

$$R_{ac} = 2\rho\frac{2}{\delta w} \quad (\Omega/\text{m}) \tag{31.129}$$

Characteristic impedance, Z

The characteristic impedance *Z* of the go-and-return bus bar arrangement is given by

$$Z = \sqrt{\frac{R + j\omega L}{G + j\omega C}} \quad (\Omega) \tag{31.130}$$

When the conductor resistance *R* and insulation conductance *G* are negligible

$$Z = \sqrt{\frac{L}{C}} \quad (\Omega) \tag{31.131}$$

This equation illustrates that increasing the capacitance and decreasing the inductance reduces bus bar noise problems. Common to decreased inductance and increased capacitance are

- decrease the dielectric thickness *d* and
- increase the bus bar width *w*
- increase permittivity and decrease permeability

That is, characteristic impedance *Z* is proportional to *d/w*.

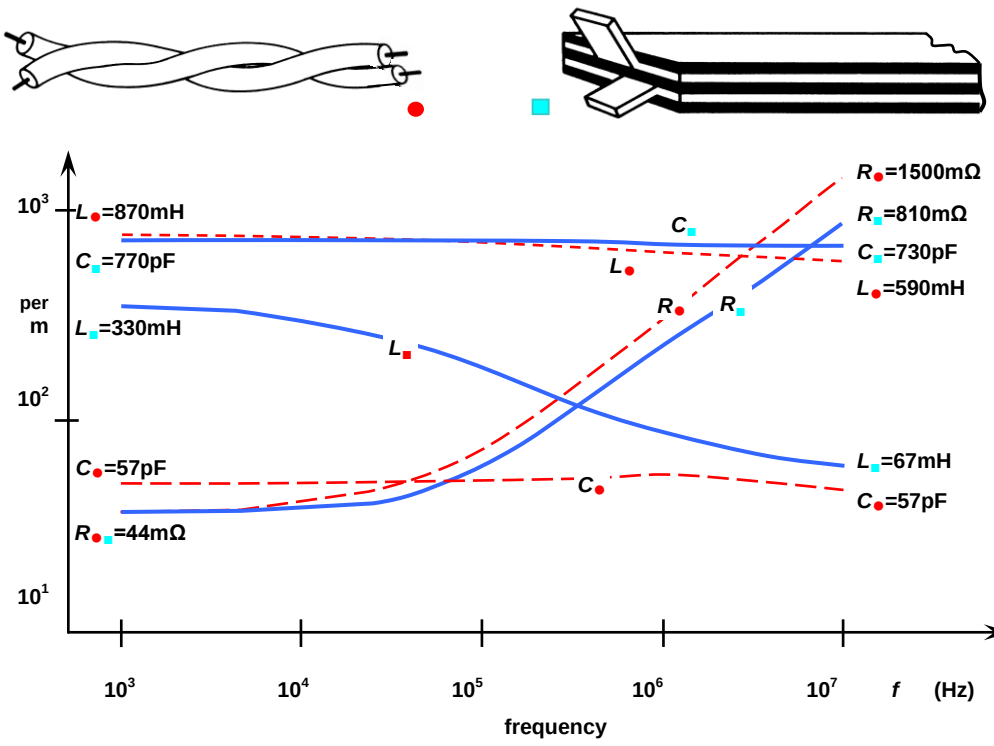

Figure 31.28. *Comparison between electrical parameters for a twisted pair and a laminated bus bar, each with the same copper cross sectional area, that is, the same dc resistance.*

Figure 31.28 compares the electrical parameters obtained for one metre of twist pair plastic coated 1mm diameter solid copper wire and one metre of laminated bus bar. The copper cross section area is the same in each case, giving a dc resistance of 44mΩ per metre. The most significant electrical factor is the reduction in inductance when a bus bar arrangement is used. Better electrical parameters are gained for a significant cost increase.
The propagation delay time is approximately

$$t_{pd} = 0.04 \times C \times Z \qquad (\text{ps/mm}) \qquad (31.132)$$

31.15 Appendix: Insulating material for between bus bar conductors

If the busbar is to be edge filled, epoxy glass is recommended for the top and bottom insulators. If it is to be sealed by pinching off the insulation, Nomex type materials are recommended.

Material	Minimum thickness	K-factor	Dielectric strength
	mil	pu	kV/mil
Mylar	2	3.3	7.5
Epoxy glass	2.5	4.3	0.5
Kapton	1	3.8	4.6
Nomex	3	2.6	0.5

31.16 Appendix: Materials by types of magnetization

Diamagnetic: Ordering magnetic particles are electron pairs or magnetic nuclei. They are ordered in one direction under external magnetic field. Materials exhibit magnetization opposing to the applied magnetic field. Magnetic field is weakened in a material. Weak repelling effect to the magnetic field. The value of susceptibility is independent of temperature. Magnetization disappears when the field is removed. *Example* - most objects around - wood.

Paramagnetic: Ordering magnetic particles are unpaired electrons (spins). The magnetic moments tend to be randomly orientated due to thermal fluctuations when there is no magnetic field. They are ordered in one direction under external magnetic field such that magnetisation of the material is proportional to the applied field. Materials exhibit magnetization reinforcing (parallel, therefore - para) to the applied magnetic field. Magnetic field is strengthened in a material. Weak attracting effect to the magnetic field. Magnetization disappears when the field is removed. *Example* - aluminium metal (Al).

Ferromagnetic: Ordering magnetic particles are unpaired electrons (spins). They are ordered in one direction under external magnetic field. Below Curie point, ferromagnets exhibit magnetization without of any external magnetic field (spontaneous magnetization) due to self-ordering of spins. Exhibit reinforcing magnetization to the applied magnetic field that usually remains when the field is removed (field-induced magnetization). Magnetic field is strengthened in a material. Strong attracting effect to the magnetic field. In the periodic table of elements only Fe, Co and Ni are ferromagnetic at and above room temperature. As ferromagnetic materials are heated then the thermal agitation of the atoms means that the degree of alignment of the atomic magnetic moments decreases and hence the saturation magnetisation also decreases. Eventually the thermal agitation becomes so great that the material becomes paramagnetic; the temperature of this transition is the Curie temperature, T_C (Fe: T_C =770°C, Co: T_C =1131°C and Ni: T_C =358°C). *Example* - iron metal (Fe).

Antiferromagnetic: Ordering magnetic particles are unpaired electrons (spins). In contrast to paramagnetic and ferromagnetic, they are ordered in opposite directions in equal quantities under the action of magnetic field and since the field cancels out, the material appears to behave in the same way as a paramagnetic material. The ordering usually remains when the field is removed. Like ferromagnetic materials these materials become paramagnetic above a transition temperature, known as the Néel temperature, T_C. (Cr: T_N = 37ºC). Below Neel point, self-ordering can be observed. Magnetic field is weakened in a material. Weak repelling effect to the magnetic field. In the periodic table the only element exhibiting antiferromagnetism at room temperature is chromium. *Example* - nickel oxide (Ni0).

Ferrimagnetic: Ferrimagnetism is only observed in compounds, which have more complex crystal structures than pure elements. Ordering magnetic particles are unpaired electrons (spins). They are ordered in opposite directions in unequal quantities/sizes under the action of magnetic field. Behave as weak ferromagnets. Magnetic field is strengthened in a material. Weak to strong attracting effect to the magnetic field. *Example* - magnetite (Fe_3O_4).

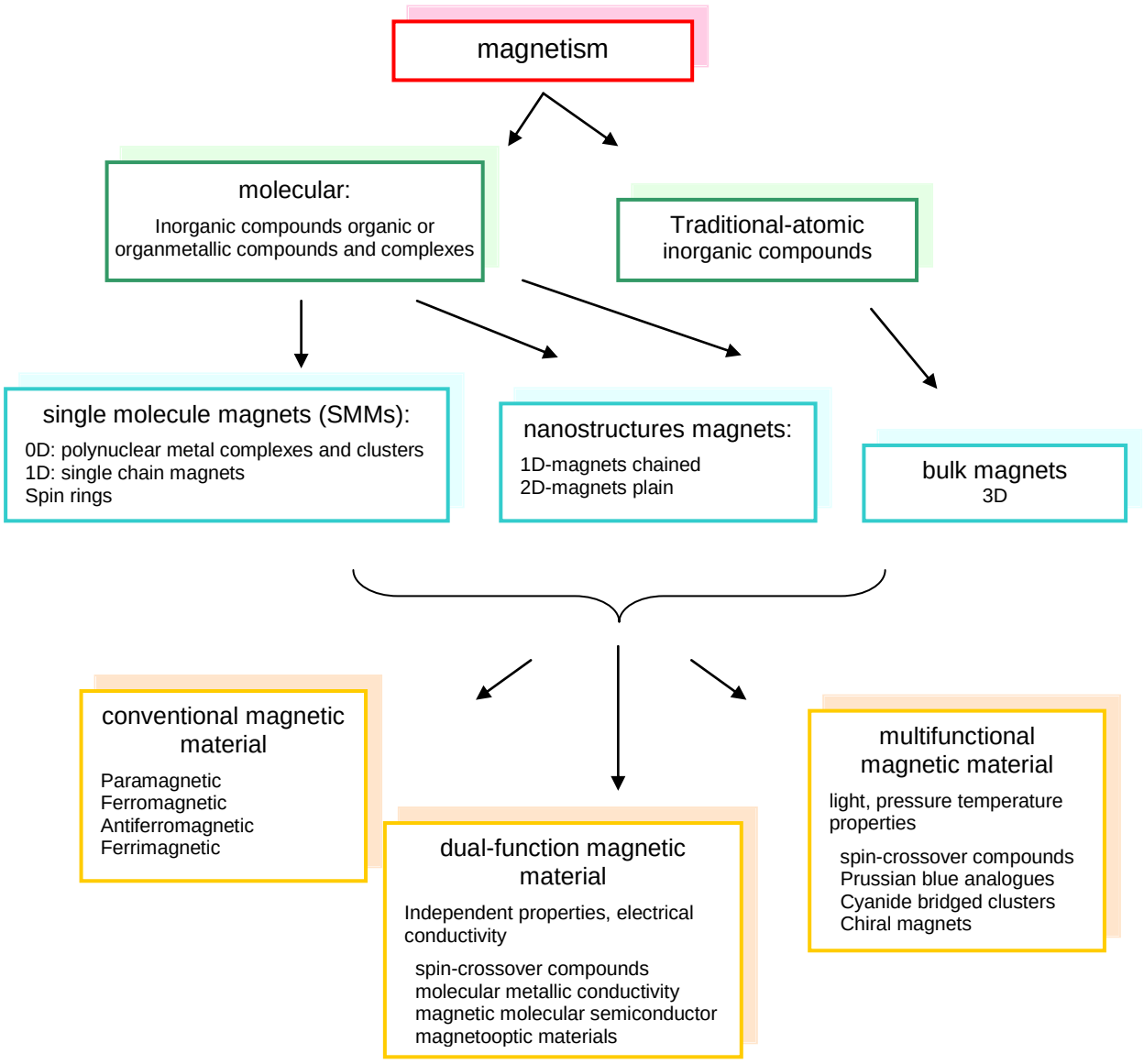

Figure 31.29. *Classification of magnetic materials.*

Metamagnetic: Materials that can change their magnetic properties depending on the strength of applied magnetic field. For example, paramagnets transform to ferromagnets or vice versa when the field is increased or reduced.

Magnetic materials - structural types

Figure 31.29 classifies development in both inorganic and organic magnetic materials
Relatively recently, the science of so-called molecular magnetism branched out from traditional magnetism that explored mainly magnetic behaviour of compounds at the level of atoms (in metals). Molecular magnetism researches magnetic behaviour of molecules rather than atoms. Magnetic behaviour of organic compounds belongs to the field of molecular magnetism.
Molecules as well as atoms may form bulk magnets (traditional type of magnets), that are also known as 3D magnets. At the same time, two new types of molecular magnets recently evolved: single molecule magnets (SMMs) and nanostructured magnets.
SMMs are fully functional magnets on a molecular level. They possess some unique properties, such as quantum tunnelling of magnetization. SMMs include: polynuclear metal complexes and clusters, single-chain magnets, spin rings and some others.
Nanostructured magnets built of self-organized or self-assembled crystallites. They may possess many unique properties in addition to magnetic ones, (such as anisotropy, transparency, electrical conductance, porosity etc.). Low dimensionality (0D, 1D, 2D) is characteristic of self-aggregated molecular magnets.
Bulk molecular (and atomic) magnets usually contain materials that may be either paramagnetic, ferromagnetic, anti-ferromagnetic, or ferrimagnetic. Recently, a new type of molecular magnetic

materials evolved, that may change magnetic properties under the action of different external factors, such as light, temperature, pressure, etc. They are known as multifunctional magnetic materials, which include so-called spin-crossover compounds, Prussian Blue analogues, cyanide-bridged clusters, chiral magnets.
The other type of new functional molecular magnetic materials are dual-function materials. They possess one or more independent physical properties in addition to magnetic properties, such as electrical conductivity, porosity, or optical properties. Magnetic molecular conductors are the most widely studied organic materials of this type.

31.17 Appendix: Magnetic behaviour of stainless steels

The magnetic properties of stainless steels vary considerably, ranging from paramagnetic, non-magnetic, in fully austenitic grades to hard or permanent magnetic behaviour in the hardened martensitic grades.

Austenitic (non-magnetic) Stainless Steels
All austenitic stainless steels are paramagnetic, non-magnetic, in the fully austenitic condition as occurs in well-annealed alloys. The dc magnetic permeabilities range from 1.003 to 1.005 when measured with magnetizing forces of 16 kA/m. The permeability increases with cold work due to deformation-induced martensite, a ferromagnetic phase. For certain grades such as Types 302 and 304, the increase in magnetic permeability can be appreciable, resulting in them being weakly ferromagnetic in the heavily cold-worked state. For example, Type 302 and 304 increase in permeability by ten fold when the cold reduction is 80%.
The magnetic permeabilities achievable in austenitic stainless steels are low compared to conventional magnetic materials. Consequentially, their non-magnetic behaviour is of more concern.
Austenitic stainless steels are not hardenable by heat treatment. If the application requires that the steel be hardenable, use Martensitic and precipitation hardenable stainless steels, below; however, they are ferromagnetic. It is important to consider the effects of using ferromagnetic materials in magnetic circuits if the circuit was originally designed using paramagnetic steels.

Examples of austenitic stainless steels are Type 302, 303, 304, 316, and 316L.

Ferritic Stainless Steels
Ferritic stainless steels are ferromagnetic and can be used as soft magnetic components such as solenoid cores, pole pieces and return paths. Although their magnetic properties are not generally as good as conventional soft magnetic alloys, they are successfully used for magnetic components that must withstand corrosive environments. As such, they offer a cost-effective alternative to plated iron and silicon-iron components. Additionally, the relatively high electrical resistivity of ferritic stainless steels results in excellent AC performance.
These stainless steels have soft magnetic properties: high magnetic permeability, low coercive force, H_c, and low residual induction B_r, which depend on alloy chemistry. In particular, impurities such as carbon, sulphur, and non-metallic inclusions, and stresses due to cold working. Magnetic permeability decreases and the coercive force increases; the behaviour is less magnetically soft with increasing amounts of impurities and stress. Hence, optimum magnetic performance is obtained with well-annealed, high-purity alloys. Carpenter 430F and 430FR (Solenoid Quality) is an excellent choice for soft magnetic alloy applications. Note that if the material has been cold worked, its coercivity, H_c, will increase, and when exposed to magnetic fields, it will retain some magnetic effects, hence acting as a weak permanent magnet.

Examples of Ferritic stainless steel are Type 430F Solenoid Quality, 430FR Solenoid Quality, and 446.

Martensitic and Precipitation Hardenable Stainless Steels
All Martensitic and most precipitation hardenable stainless steels are ferromagnetic. Due to the stresses induced by the hardening transformation, these grades exhibit permanent magnetic properties if magnetized in the hardened condition. For a given grade, the coercive force, H_c, tends to increase with increasing hardening, rendering these alloys more difficult to demagnetize.

Examples of martensitic stainless steels are Type 410, 416, 420, 440B, and 17-4.

Reading list

cda.org.uk (copper development agency)

EPCOS Ferrite design tool
www.epcos.com

McLyman, W. T., *Transformer and Inductor Design Handbook*,
Marcel Dekker Inc., 1978.

Snelling, E. C., *Soft Ferrites*,
Butterworth, second edition, 1988.

Manufacturers Data Handbooks, Catalogues, and www

Siemens	Thomson CSF	Philips
SEI	Telmag	Neosid
Magnetics Inc (mag-inc.com)	Krystinel Corp	Stackpole
Ferroxcube Inc	Arnold Eng. Co.	Micrometals Co.
Pyroferric Inc	Fuji	Fair-rite

Hitachi Metals http://www.hitachi-metals.co.jp/e/

Vacuumschmelze http://www.vacuumschmelze.de/dynamic/en/

Mecagis http://www.mecagis.com/index.php

Magnetec http://www.magnetec.de/magnetec.htm

Problems

31.1. Rework example 31.7, taking B_r = 0.18 T into account.

31.2. Rework example 31.7, when the core temperature is 100°C.

31.3. Rework example 31.3 when
$V_e = 7.3 \times 10^{-6}$ m^3 $A_e = 66$ mm^2
$\ell_e = 110$ mm $c = 0.75$ nH
What are the effects of decreasing the core volume for a given L and I?
[10A: 274 J/m^3, 0.53 mm, 1200 A/m, 13 turns; 20A: 2360 A/m, μ_e = 185]

31.4. Show that the maximum flux density for a square-wave-excited transformer is given by

$$\hat{B} = \frac{V}{4NAf}$$

31.5. A 2:1 step-down transformer with an effective area of 10 cm^2 is driven from a 240V, 1kHz square-wave source. The transformer has 240 primary turns and magnetising inductance of 10mH.
i. Calculate the maximum flux density.
ii. Calculate the peak primary current when the secondary is loaded with a 5Ω resistor. Sketch the primary and secondary current waveforms.
[0.25 T, 30 A]

blank